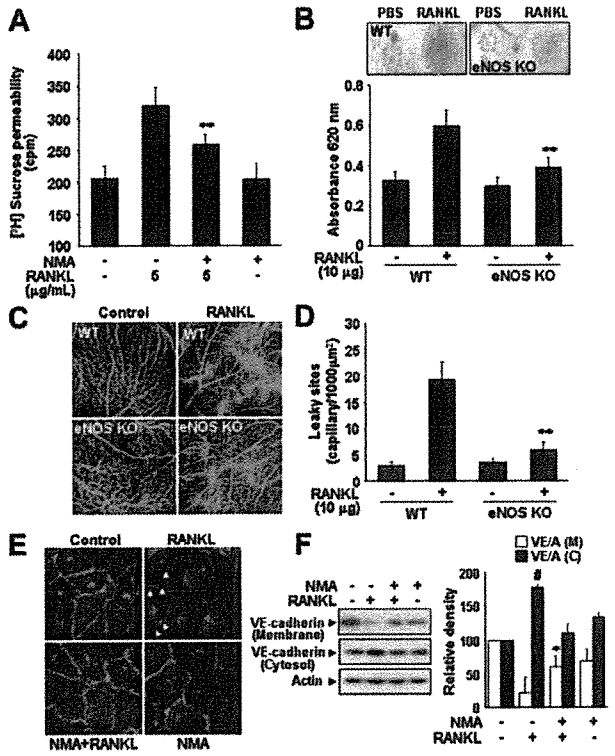

Figure 2. Impairment of RANKL-induced vascular hyperpermeability in eNOS-deficient mice. (A) HUVECs were preincubated for 30 minutes with or without NMA (1 mM) and stimulated with 5 μg/mL RANKL for 1 hour. A [³H]sucrose permeability assay was then performed. Three independent experiments were performed in duplicate. Data are means ± SEs; $^{**}P < .01$ versus RANKL alone. (B) An in vivo Miles vascular permeability assay was performed in WT and eNOS KO mice (n = 7 per group) as described in Figure 1. Data are means ± SDs; $^{**}P < .01$ versus RANKL in eNOS KO. (C) Representative fluorescence images of retinal vessels. RANKL (10 μg) or PBS was injected into the vitreous cavity of WT and eNOS KO mice (n = 7 per group). After 24 hours, the mice received an intravenous injection of 10 mg FITC-dextran (MW = 20 000 D), and their retinas were flat-mounted. (D) The vascular permeability was quantified by counting sites with extravasation of fluorescence at postcapillary vessel. Data are means ± SDs; $^{**}P < .01$ versus RANKL in eNOS KO. (E-F) HUVECs were preincubated for 30 minutes with or without NMA (1 mM) and stimulated with 5 μg/mL RANKL for 1 hour. (E) An immunofluorescence analysis of VE-cadherin. Arrows indicate disruption of VE-cadherin. (F) Translocation of VE-cadherin was assessed as described in "Materials and methods." The Triton X-100–insoluble and soluble fractions were subjected to SDS–polyacrylamide gel electrophoresis followed by Western blot analysis with anti–VE-cadherin. Blots are representative of 3 independent experiments. Densitometric analyses are presented as the relative ratio of VE-cadherin to actin. VE indicates VE-cadherin; A, actin; M, membrane; C, cytosol. Data are means ± SDs; $^{*}P < .05$ versus RANKL alone; $\#P < .05$ versus untreated control.

significantly abrogated RANKL-induced endothelial permeability in vitro (Figure 2A). Consistently, vascular hyperpermeability of the mouse skin by RANKL was substantially impaired in the eNOS KO mice compared with WT mice (Figure 2B). We further investigated the role of eNOS in retinal vascular permeability that is caused by breakdown of tight junctions between the retinal vascular endothelial cells. As shown in Figure 2C-D, injection of RANKL into the vitreous cavity of WT mice induced marked retinal vascular leakage as evidenced by the widespread, diffuse fluorescence. By contrast, the retinal vessels of the eNOS KO mice remained clearly delineated, with little or no leakage. Furthermore, the effect of RANKL on leukocyte extravasation in vivo was significantly abrogated in eNOS KO mice compared with WT mice (Figure S1A-B, available on the *Blood* website; see the Supplemental Figures link at the top of the online article).

Vascular endothelial permeability is maintained by the endothelial junction proteins, VE-cadherin, and occludin.[24] The effect of RANKL on adherens junction (AJ) formation was examined by immunostaining with anti–VE-cadherin. In confluent ECs, VE-cadherin is located at cell-cell contacts. When HUVECs were treated with RANKL, the level of VE-cadherin at cell-cell junctions markedly decreased, and pretreatment with NMA blocked this effect (Figure 2E). Normally, VE-cadherin that is anchored to the actin cytoskeleton is detected in the detergent-insoluble fractions of cell lysates.[25] There was a decrease in VE-cadherin in the Triton X-100–insoluble fraction and a concomitant increase in the Triton X-100–soluble fraction after stimulation with RANKL. This effect was reversed by NMA (Figure 2F). Taken together, these results demonstrate that RANKL induces vascular hyperpermeability in an NO-dependent manner by promoting the breakdown of endothelial AJs.

RANKL induces eNOS activation and NO production via a TRAF6/PI3K/Akt signaling pathway

To confirm whether RANKL stimulates NO production in endothelial cells, quiescent HUVECs were stimulated with RANKL and assayed for NO production and eNOS activity. RANKL increased NO production and eNOS activity (Figure 3A-B), without affecting the expression of eNOS protein (Figure 3C). The eNOS activity was evidently increased at 0.5 hours after RANKL treatment and sustained up to 24 hours (Figure 3B). eNOS is an isoform of NO synthase that is constitutively expressed in HUVECs and activated

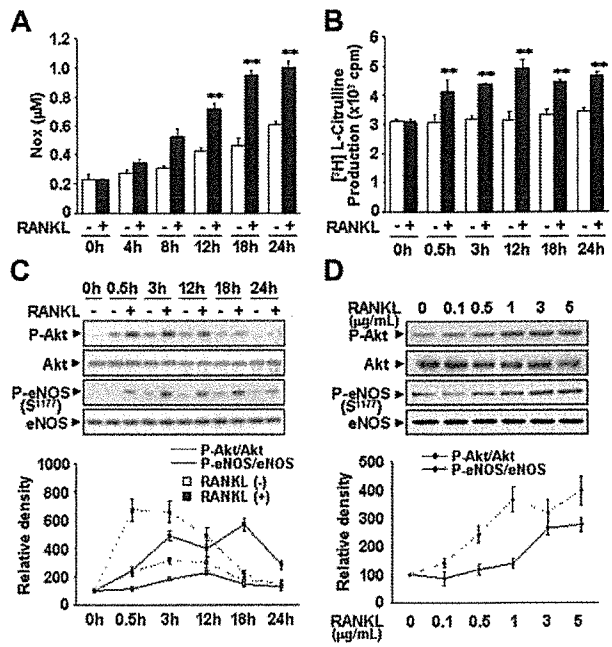

Figure 3. RANKL induces eNOS activation and NO production in endothelial cells. (A-D) HUVECs were stimulated with 5 μg/mL RANKL for the indicated times (A-C) and with various concentrations of RANKL for 30 minutes (D). (A) Levels of NOx was determined in the culture medium by using a chemiluminescent NO analyzer. (B) The eNOS enzymatic activity was measured by the production of [³H]-L-citrulline from [³H]-L-arginine. Three independent experiments were performed in duplicate. Data are means ± SEs. Statistical analysis of the results was carried out using ANOVA. $^{**}P < .01$ versus untreated control in 0 hour and each time point. (C-D) The levels of eNOS protein and phosphorylation of Akt and eNOS by RANKL were determined by Western blotting (top). Blots are representative of 3 independent experiments. Densitometric analyses are presented as the relative ratio of P-Akt to Akt and P-eNOS to eNOS. The relative ratio in untreated control is arbitrarily presented as 100 (bottom).

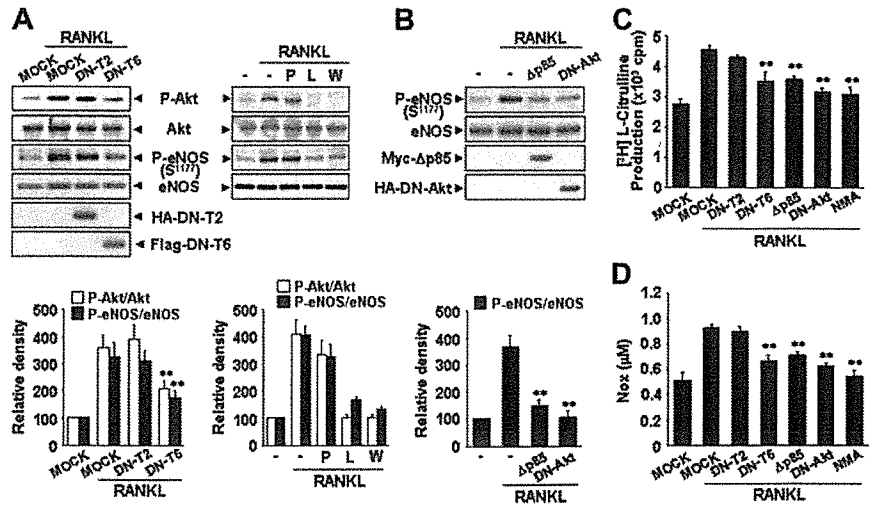

Figure 4. RANKL induces eNOS activation and NO production via a TRAF6/PI3K/Akt signaling pathway. (A) HUVECs were stably transfected with a HA-tagged DN-T2 and a Flag-tagged DN-T6 using retroviral system (left). HUVECs were preincubated for 30 minutes with or without 5 μM PP1, 100 nM Wortmannin, or 1 mM NMA prior to stimulation with RANKL (5 μg/mL) for 20 minutes (right). (B) HUVECs were transiently transfected with a HA-tagged DN-Akt or a Myc-tagged Δp85. (A-B) The levels of eNOS protein and the phosphorylation of Akt and eNOS by RANKL were determined by Western blotting (top). Blots are representative of 3 independent experiments. Densitometric analyses are presented as the relative ratio of P-Akt to Akt and P-eNOS to eNOS (bottom). (C-D) eNOS activity and NO production were measured as described in Figure 3A-B. Three independent experiments were performed in duplicate. Data are means ± SDs; $^{**}P < .01$ versus RANKL alone.

by Akt-mediated phosphorylation at Ser1177.[26,27] When HUVECs were exposed to RANKL, there was a dose-dependent increase in phosphorylation of eNOS at Ser1177 (Figure 3D). The increase was detected within 10 minutes, reached a maximum at 20 to 30 minutes, and was sustained for nearly 24 hours (Figure 3C). Consistent with this, we detected an increase in Akt phosphorylation (Figure 3C-D). However, other phosphorylation sites of eNOS were not changed by RANKL treatment (Figure S2).

We further analyzed the signaling mechanism involved in RANKL-induced eNOS phosphorylation and NO production. RANK, like other TNFR family members, lacks catalytic activity and interacts with TRAFs that act as adaptors activating downstream signaling pathways. Of the TRAFs, TRAF2 and TRAF6 appear to be important components of the RANKL signaling pathway.[28] Overexpression of DN-T6 resulted in substantial inhibition of eNOS phosphorylation, eNOS activity, and NO production, whereas DN-T2 had no effect (Figure 4A,C-D). Recruitment of TRAF6 to the cytoplasmic domains of RANK can lead to the activation of PI3K that subsequently links to Akt pathway. Indeed, the PI3K inhibitors, LY294002 and Wortmannin, markedly inhibited RANKL-induced eNOS phosphorylation, whereas PP1, a potent Src tyrosine kinase inhibitor, had no effect (Figure 4A). Consistently, overexpression of Δp85, a dominant-negative mutant of the p85 regulatory subunit of PI3K, and DN-Akt, a dominant-negative mutant of Akt, inhibited RANKL-induced eNOS activation (Figure 4B-D). Taken together, these results indicate that RANKL stimulates the production of endothelial NO via a TRAF6-dependent PI3K/Akt signaling pathway acting on eNOS.

NO is required for RANKL-induced migration and capillary-like network by ECs

RANKL induced the formation of extensive capillary-like networks of ECs cultured on 2-D Matrigel matrix, and this effect was almost completely inhibited by pretreatment with NMA (Figure 5A-B). Consistent with involvement of the eNOS activation pathway, RANKL-induced capillary-like network was blocked by Wortmannin, as well as by overexpression of DN-T6, but not of DN-T2 (Figure 5C-D). We next examined the role of NO in RANKL-induced EC migration. RANKL stimulated the chemotactic motility of HUVECs approximately 1.5-fold, and this effect was abolished by Wortmannin and NMA, as well as by DN-T6 (Figure

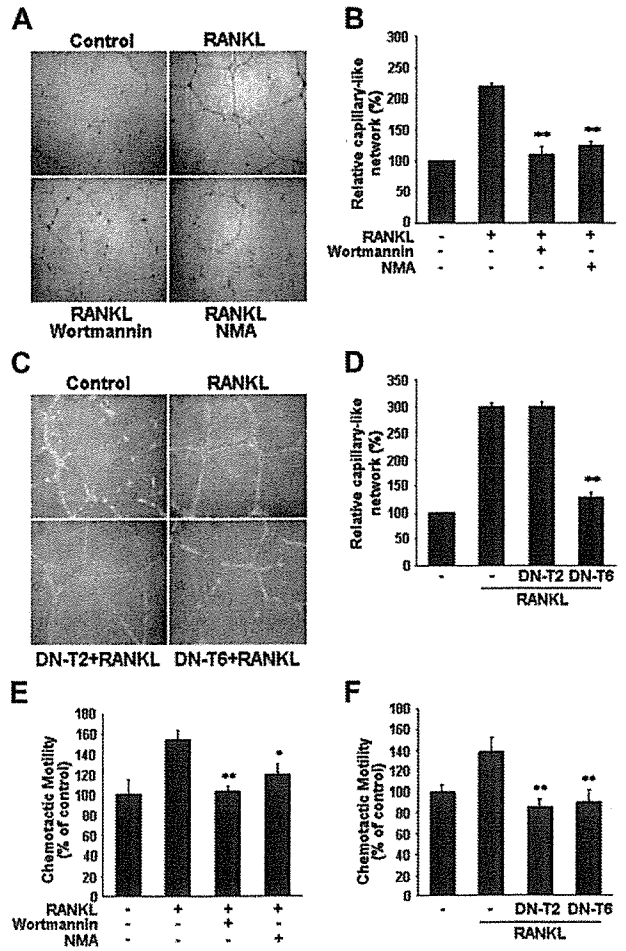

Figure 5. Involvement of PI3K/Akt-dependent NO production in RANKL-induced migration and capillary-like network by ECs. (A,E) HUVECs were preincubated for 30 minutes with or without 100 nM Wortmannin or 1 mM NMA prior to stimulation with RANKL (5 μg/mL). (C, F) HUVECs were stably transfected with DN-T2 and DN-T6 using retroviral system. (A,C) Cells were plated on Matrigel-coated plates at a density of 2×10^5 cells/well and incubated with 5 μg/mL RANKL. Microphotographs were taken after 20 hours (× 200). (B,D), Capillary-like networks were quantified with Image-Pro Plus software. (E-F) After 4 hours of incubation, chemotaxis was quantified with an optical microscopy. Three independent experiments were performed in duplicate. Data are means ± SDs; $^{*}P < .05$; $^{**}P < .01$ versus RANKL alone.

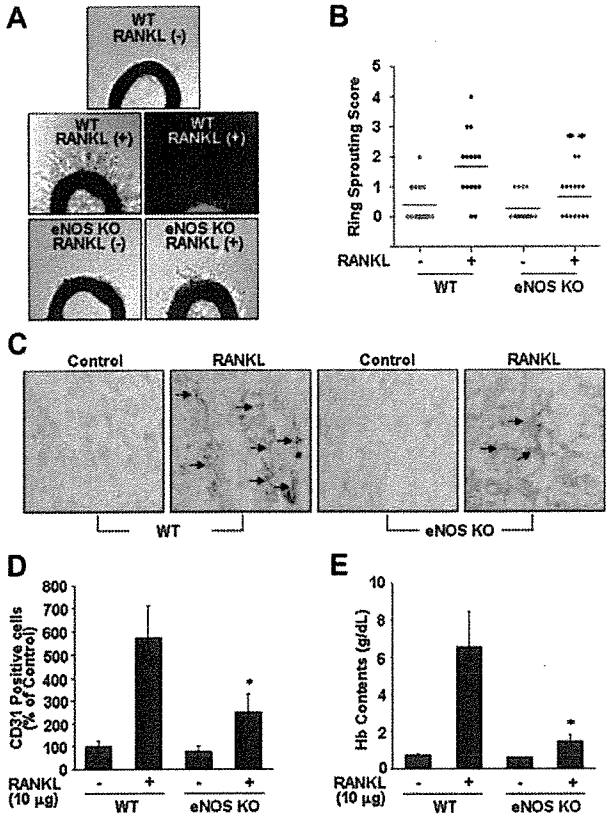

Figure 6. eNOS plays a critical role in RANKL-induced angiogenesis. (A) Aortic segments were harvested from WT and eNOS KO mice (n = 7 per group). Endothelial-cell sprouts forming branching cords from the margins of vessel segments taken from mice were photographed under a phase microscope. Staining of endothelial cells sprouted from RANKL-treated aorta with VWF (middle). (B) Sprouting scores were classified from 0 (least positive) to 5 (most positive). Data are means ± SEs. (C-E) WT and eNOS KO mice (n = 7 per group) were injected with 0.6 mL Matrigel containing RANKL (10 μg). After 7 days, the mice were killed and the Matrigel plugs were excised. (C) Plugs were stained for infiltrating endothelial cells using anti-CD31 antibody. Arrows indicate $CD31^+$ cells. (D) Quantitative assessment of $CD31^+$ endothelial cells. (E) Quantification of neovessel formation by measuring hemoglobin in the Matrigel. Data are means ± SDs; $^*P < .05$; $^{**}P < .01$ versus RANKL in WT.

5E-F). These results suggest that NO is required for the migration and differentiation of ECs in response to RANKL. In contrast to its lack of effect on EC capillary-like network, DN-T2 did inhibit the RANKL-induced increase in chemotactic motility of the HUVECs (Figure 5F), pointing to the involvement of NO-independent pathways activated by TRAF2 in RANKL-induced EC migration.

eNOS plays a critical role in RANKL-induced angiogenesis

To further assess the role of NO in RANKL-induced angiogenesis, we compared endothelial-cell sprouting in the aortic ring segments from eNOS KO and WT mice. RANKL caused a 3-fold increase in endothelial-cell sprouting in WT mice, but this effect was significantly abrogated in the aortic rings from eNOS KO mice (Figure 6A-B). Furthermore, RANKL-induced sprouting of endothelial cells in the rat aortic rings was stimulated by RANKL, and this angiogenic response was inhibited by simultaneous treatment with Wortmannin or NMA (Figure S3A-B). We further analyzed the role of endothelial cell–derived NO in RANKL-induced neovascularization in vivo. Matrigel containing RANKL was subcutaneously injected into WT and eNOS KO mice, and 7 days later the Matrigel plugs formed in the mice were excised and analyzed. There was nearly 70 g/L (7 g/dL) hemoglobin in the plugs of the WT mice, whereas those of the KO mice contained only about 18 g/L (1.8 g/dL) (Figure 6E). Plugs of the WT mice exhibited significantly higher densities of $CD31^+$ endothelial cells than those of KO mice (Figure 6C-D). Consistently, in a corneal micropocket assay, RANKL was less angiogenic in the eNOS KO mice than in the WT mice as measured by the numbers of neovessels (Figure S4A-B).

Discussion

The present results have revealed a novel action of RANKL, namely that of increasing vascular permeability in vitro and in vivo. Moreover RANKL can be added to the list of NO-dependent endothelial stimuli that promote both vascular leakage and angiogenesis. Our findings have implications for the role of RANKL in vascular physiology. Given its considerable adverse effects in adults, such as arterial calcification and inflammatory activation enhancing leukocyte adhesiveness,[5,29] our findings underline the possibility that RANKL is implicated in the development of vascular diseases.

Atherosclerosis has many characteristics in common with inflammatory disease characterized by infiltration of activated immune cells into the intima.[30] We have recently demonstrated that RANKL causes adhesion of leukocytes to ECs as a consequence of increased expression of cell adhesion molecules such as ICAM-1 and VCAM-1 in the ECs.[29] RANKL is produced by various cells, including vascular cells and activated immune cells close to blood vessels, and it exists in either a cell-bound or a secreted form.[3] Its expression, together with OPG, is also modulated by various factors such as the inflammatory cytokines, TNF-α and IL-1β.[3] Under some circumstances, the ratio of RANKL to OPG in the vascular area increases, and this change may activate endothelial cells, which are thought to be involved in promoting the early stage of atherosclerotic inflammation, which is characterized by increased endothelial permeability, up-regulation of adhesion molecules, and transendothelial migration of leukocytes.[31,32] Moreover, considering that angiogenesis and calcification are common features of advanced atherosclerotic lesions, the angiogenic and calcifying activities of RANKL may contribute to the development of atheromatous vessels.[33] Notably, this notion was supported by recent studies showing the enhanced expression of RANKL both in clinical and experimental atherosclerosis.[8] mRNA levels of RANKL were increased in T cells in patients with unstable angina accompanied by increased expression of RANK in monocytes.[8] In the $apoE^{-/-}$ mice, RANKL is significantly expressed within the atherosclerotic plaques, whereas no RANKL immunostaining was detected in the nonatherosclerotic vessel wall.[8] Furthermore, Bennett et al[9] have demonstrated that OPG inactivation results in larger and more calcified advanced lesions in the innominate arteries of older $apoE^{-/-}$ mice.

Vascular permeability is defined as the movement of fluids and molecules between blood vessels and the underlying tissues, and it is regulated by various inflammatory factors that break down intercellular endothelial junctions.[34] Although vascular leakage is not a prerequisite for blood vessel growth, increased vascular permeability often coincides with the early stage of angiogenesis and is also found in areas of diseased tissue in diabetic retinopathy, solid tumors, myocardial infarction, wounds, and chronic inflammation.[35] VEGF, originally isolated as a vascular permeability factor (VPF), is the best known angiogenic stimulus increasing the

vascular permeability of microvessels to circulating macromolecules.[16] This VPF activity is correlated with various vascular pathophysiologies.[34] In contrast, endothelial permeability is not directly affected by bFGF and PDGF, or inhibited by angiopoietin-1, despite their prominent angiogenic activities.[35,36] Our data show that the effect of RANKL on endothelial permeability is comparable to that of VEGF. Because RANKL does not increase VEGF expression in ECs,[13] RANKL-induced endothelial permeabilization and angiogenesis appear to be exerted by a direct action on ECs, independent of VEGF. Note that injection of RANKL, like VEGF, into the vitreous cavity causes breakdown of the blood-retinal barrier formed by tight junctions between the retinal vascular endothelial cells, even though the mode of action of RANKL on the retinal vasculature is unknown.

It is interesting that the effects of RANKL on ECs are so similar to those of VEGF. VEGF was originally isolated from the vasculature and was shown to play essential roles in vascular physiology during embryonic development, as well as in the evolution of various diseases of adult vasculature. It has been found that VEGF is also capable of directly enhancing osteoclastic bone resorption and promoting the survival of mature osteoclasts.[37] Conversely, although RANKL was discovered as a factor active in bone remodeling, its role in vascular disease is increasingly recognized.[38] For example, inhibition of RANKL with OPG or RANK fusion proteins or RANKL antibodies reduced chronic inflammatory disorders and malignant tumors in animal models, in addition to bone loss caused by osteoporosis.[38] Our current and previous findings that RANKL promotes vascular permeabilization, angiogenesis,[13] and proinflammatory activation provide further evidence of the adverse effects of RANKL on adult vasculature.[29]

Our data also demonstrate the prominent roles of eNOS in RANKL-induced angiogensis and vascular permeability in vitro and in vivo. Many angiogenic factors, but not all, use NO as mediator in their angiogenic effects. Treatment of ECs with RANKL increased NO production, together with increased eNOS activity (Figure 3A-B). Blockage of NO release prevented RANKL-induced EC migration and capillary-like network formation in vitro, as well as sprouting of ECs from rat aorta (Figure 5; Figure S3). Both the mouse Matrigel plug assay and the cornea micropocket assay revealed that RANKL-induced neovascularization was substantially impaired in eNOS KO animals (Figure 6; Figure S4). Thus, it is clear that NO generated from eNOS is required for angiogenic responses to RANKL. The signaling mechanism involved in vascular permeabilization is complex and involves a wide array of factors that affect cell-cell junctions, cell-matrix interaction, and cytoskeletal organization. Involvement of protein kinase C (PKC) and Rho-mediated signaling pathways has been demonstrated in the endothelial permeability induced by various stimuli.[39] NO also seems important in mediating vascular permeability, but this is context dependent. In ischemia-reperfusion injury models, NO has been shown to maintain vessel integrity.[15] However, it increased vascular permeability in tumors and in chronic inflammation.[35] Our present data indicate that NO plays an important role in RANKL-induced vascular permeability because vascular leakage in the skin of mice and in the retina induced by RANKL was significantly reduced in eNOS KO mice, and these in vivo findings were confirmed by measuring permeability and VE-cadherin junction in cultured endothelial cells. However, RANKL-induced permeability was not completely blocked by inhibiting NO production, pointing to the contribution of other signaling components such as PKC, which is activated in ECs by RANKL.[29]

RANKL causes NO production by ECs via PI3K/Akt-dependent eNOS activation (Figure 4A-D). Although eNOS is constitutively expressed in ECs, its activity can be modulated by variation in its level of expression or by reversible phosphorylation on Ser1177.[27] Treatment of ECs with RANKL did not alter the levels of eNOS mRNA and protein (Figure 3C). However, it led to phosphorylation of eNOS at Ser1177, a major phosphorylation site for Akt, and this was blocked by a dominant-negative form of Akt. Moreover, blockage of either PI3K or Akt resulted in a significant reduction in NO production in response to RANKL. Recently, we demonstrated the involvement of Src and PLC pathway in RANKL-induced angiogenesis.[13] However, the Src inhibitor PP1 had no effect on RANKL-induced eNOS activation, indicating that Src is not upstream of the Akt/eNOS pathway by RANKL. Our data also point to a predominant role of TRAF6 in the RANKL-induced NO production. Previous studies in nonendothelial cells have shown that TRAF adaptor proteins such as TRAF2, TRAF5, and TRAF6 can associate with the cytoplasmic tail of RANK and activate various intracellular signaling pathways.[28] We have recently demonstrated that TRAF2 and TRAF6 play an important role in RANKL-induced NF-κB activation in endothelial cells, which leads to increased endothelial CAM expression and EC-leukocyte interactions.[29] Surprisingly, a dominant-negative form of TRAF6 but not of TRAF2 inhibited NO production and phosphorylation of Akt and eNOS. Because PI3K mediates Akt phosphorylation, TRAF6 probably links the membrane receptor RANK to PI3K in ECs. Therefore, these results suggest a multifaceted role of TRAF6 in the RANK-mediated angiogenic and inflammatory signaling pathways in ECs.

In summary, the present study provides the first evidence that RANKL increases endothelial permeability in addition to stimulating angiogenesis as previously shown, and it reveals that these effects are dependent on endothelium-derived NO. These findings suggest that elevated RANKL levels in the vascular area may lead directly to endothelial activation and may make an important contribution to the occurrence of angiogenesis-dependent inflammatory vascular diseases such as atherosclerosis.

Acknowledgments

This work was supported by Korea Biotech R&D Group of MoST (Ministry of Science and Technology) (research grant M10416130002-04N1613-00210), the Korea Research Foundation of Korean Government (Ministry of Education and Human Resources Development [MOEHRD]) (grant KRF-2003-C00054), Molecular Cellular Biodiscovery Research Group of MoST (grant 2004-01587), and Vascular System Research Center grant from Korean Science and Engineering Foundation (KOSEF).

Authorship

Contribution: J.-K.M. and Y.-G.K. designed the research; J.-K.M., Y.-L.C., J.-H.C., Y.K., and J.H.K. performed the research; Y.-G.K. and J.R. contributed material; J.-K.M., Y.-G.K., and Y.S.Y. collected data; J.-K.M., Y.-G.K., N.M., Y.-M.K., and G.T.O. analyzed data; and J.-K.M. and Y.-G.K. wrote the paper.

Conflict-of-interest disclosure: The authors declare no competing financial interests.

Correspondence: Young-Guen Kwon, Department of Biochemistry, College of Sciences, Yonsei University, Seoul, 120-749, Republic of Korea; e-mail: ygkwon@yonsei.ac.kr.

References

1. Folkman J. Angiogenesis in cancer, vascular, rheumatoid and other disease. Nat Med. 1995;1: 27-31.
2. Moulton KS, Heller E, Konerding MA, Flynn E, Palinski W, Folkman J. Angiogenesis inhibitors endostatin or TNP-470 reduce intimal neovascularization and plaque growth in apolipoprotein E-deficient mice. Circulation. 1999;99:1726-1732.
3. Walsh MC, Choi Y. Biology of the TRANCE axis. Cytokine Growth Factor Rev. 2003;14:251-263.
4. Sattler AM, Schoppet M, Schaefer JR, Hofbauer LC. Novel aspects on RANK ligand and osteoprotegerin in osteoporosis and vascular disease. Calcif Tissue Int. 2004;74:103-106.
5. Bucay N, Sarosi I, Dunstan C, et al. Osteoprotegerin-deficient mice develop early onset osteoporosis and arterial calcification. Genes Develop. 1998;12:1260-1268.
6. Min H, Morony S, Sarosi I, et al. Osteoprotegerin reverses osteoporosis by inhibiting endosteal osteoclasts and prevents vascular calcification by blocking a process resembling osteoclastogenesis. J Exp Med. 2000;192:463-474.
7. Collin-Osdoby P. Regulation of vascular calcification by osteoclast regulatory factors RANKL and osteoprotegerin. Circ Res. 2004;95:1046-1057.
8. Sandberg WJ, Yndestad A, Oie E, et al. Enhanced T-cell expression of RANK ligand in acute coronary syndrome: possible role in plaque destabilization. Arterioscler Thromb Vasc Biol. 2006; 26:857-863.
9. Bennett BJ, Scatena M, Kirk EA, et al. Osteoprotegerin inactivation accelerates advanced atherosclerotic lesion progression and calcification in older ApoE-/- mice. Arterioscler Thromb Vasc Biol. 2006;26:2117-2124.
10. Collin-Osdoby P, Rothe L, Anderson F, Nelson M, Maloney W, Osdoby P. Receptor activator of NF-κB and osteoprotegerin expression by human microvascular endothelial cells, regulation by inflammatory cytokines, and role in human osteoclastogenesis. J Biol Chem. 2001;276:20659-20672.
11. Kartsogiannis V, Zhou H, Horwood NJ, et al. Localization of RANKL (receptor activator of NF-κB ligand) mRNA and protein in skeletal and extraskeletal tissues. Bone. 1999;25:525-534.
12. Min JK, Kim YM, Kim YM, et al. Vascular endothelial growth factor up-regulates expression of receptor activator of NF-kappaB (RANK) in endothelial cells. Concomitant increase of angiogenic responses to RANK ligand. J Biol Chem. 2003; 278:39548-39557.
13. Kim YM, Kim YM, Lee YM, et al. TNF-related activation-induced cytokine (TRANCE) induces angiogenesis through the activation of Src and phospholipase C (PLC) in human endothelial cells. J Biol Chem. 2002;277:6799-6805.
14. Rudic RD, Shesely EG, Maeda N, Smithies O, Segal SS, Sessa WC. Direct evidence for the importance of endothelium-derived nitric oxide in vascular remodeling. J Clin Invest. 1998;101:731-736.
15. Murohara T, Asahara T, Silver M, et al. Nitric oxide synthase modulates angiogenesis in response to tissue ischemia. J Clin Invest. 1998; 101:2567-2578.
16. Fukumura D, Gohongi T, Kadambi A, et al. Predominant role of endothelial nitric oxide synthase in vascular endothelial growth factor-induced angiogenesis and vascular permeability. Proc Natl Acad Sci U S A. 2001;98:2604-2609.
17. Jaffe EA, Nachman RL, Becker CG, Minick CR. Culture of human endothelial cells derived from umbilical veins. Identification by morphologic and immunologic criteria. J Clin Invest. 1973;52:2745-2756.
18. Wong BR, Rho J, Arron J, et al. TRANCE is a novel ligand of the tumor necrosis factor receptor family that activates c-Jun N-terminal kinase in T cells. J Biol Chem. 1997;272:25190-25194.
19. Lee OH, Kim YM, Lee YM, et al. Sphingosine 1-phosphate induces angiogenesis: its angiogenic action and signaling mechanism in human umbilical vein endothelial cells. Biochem Biophys Res Commun. 1999;264:743-750.
20. Oura H, Bertoncini J, Velasco P, Brown LF, Carmeliet P, Detmar M. A critical role of placental growth factor in the induction of inflammation and edema formation. Blood. 2003;101:560-567.
21. Braman RS, Hendrix SA. Nanogram nitrite and nitrate determination in environmental and biological materials by vanadium (III) reduction with chemiluminescence detection. Anal Chem. 1989; 61:2715-2718.
22. Drabkin DS, Ausin JH. Spectrophotometric constants for common hemoglobin derivatives in human, dog, and rabbit blood. J Biol Chem. 1932; 98:719-725.
23. Min JK, Lee YM, Kim JH, et al. Hepatocyte growth factor suppresses vascular endothelial growth factor-induced expression of endothelial ICAM-1 and VCAM-1 by inhibiting the nuclear factor-kappaB pathway. Circ Res. 2005;96:300-307.
24. Bazzoni G, Dejana E. Endothelial cell-to-cell junctions: molecular organization and role in vascular homeostasis. Physiol Rev. 2004;84:869-901.
25. Lee MJ, Thangada S, Claffey KP, et al. Vascular endothelial cell adherens junction assembly and morphogenesis induced by sphingosine-1-phosphate. Cell. 1999;99:301-312.
26. Shiojima I, Walsh K. Role of Akt signaling in vascular homeostasis and angiogenesis. Circ Res. 2002;90:1243-1250.
27. Dimmeler S, Fleming I, Fisslthaler B, Hermann C, Busse R, Zeiher AM. Activation of nitric oxide synthase in endothelial cells by Akt-dependent phosphorylation. Nature. 1999;399:601-605.
28. Chung JY, Park YC, Ye H, Wu H. All TRAFs are not created equal: common and distinct molecular mechanisms of TRAF-mediated signal transduction. J Cell Sci. 2002;115:679-688.
29. Min JK, Kim YM, Kim SW, et al. TNF-related activation-induced cytokine (TRANCE) enhances leukocyte adhesiveness; induction of ICAM -1 and VCAM-1 via TRAF and PKC-dependent NF-κB activation in endothelial cells. J Immunol. 2005;175:531-540.
30. Glass CK, Witztum JL. Atherosclerosis. the road ahead. Cell. 2001;104:503-516.
31. Ross R. Atherosclerosis—an inflammatory disease. N Engl J Med. 1999;340:115-126.
32. Crotti T, Smith M, Hirsch R, et al. Receptor activator NF-κB ligand (RANKL) and osteoprotegerin (OPG) protein expression in periodontitis. J Periodont Res. 2003;38:380-387.
33. Collett GD, Canfield AE. Angiogenesis and pericytes in the initiation of ectopic calcification. Circ Res. 2005;96:930-938.
34. Weis SM, Cheresh DA. Pathophysiological consequences of VEGF-induced vascular permeability. Nature. 2005;437:497-504.
35. Fukumura D, Yuan F, Endo M, Jain RK. Role of nitric oxide in tumor microcirculation. Blood flow, vascular permeability, and leukocyte-endothelial interactions. Am J Pathol. 1997;150:713-725.
36. Thurston G, Rudge JS, Ioffe E, et al. Angiopoietin-1 protects the adult vasculature against plasma leakage. Nat Med. 2000;6:460-463.
37. Nakagawa M, Kaneda T, Arakawa T, et al. Vascular endothelial growth factor (VEGF) directly enhances osteoclastic bone resorption and survival of mature osteoclasts. FEBS Lett. 2000;473:161-164.
38. Hofbauer LC, Schoppet M. Clinical implications of the osteoprotegerin/RANKL/RANK system for bone and vascular diseases. JAMA. 2004;292: 490-495.
39. Mehta D, Rahman A, Malik AB. Protein kinase C-alpha signals rho-guanine nucleotide dissociation inhibitor phosphorylation and rho activation and regulates the endothelial cell barrier function. J Biol Chem. 2001;276:22614-22620.

Molecular Biology of the Cell
Vol. 18, 119–128, January 2007

Akt–PDK1 Complex Mediates Epidermal Growth Factor-induced Membrane Protrusion through Ral Activation

Hisayoshi Yoshizaki,*† Naoki Mochizuki,* Yukiko Gotoh,‡ and Michiyuki Matsuda†

*Department of Structural Analysis, National Cardiovascular Center Research Institute, Osaka 565-8565, Japan; †Department of Pathology and Biology of Diseases, Graduate School of Medicine, Kyoto University, Kyoto 606-8501, Japan; and ‡Institute of Molecular and Cellular Biosciences, University of Tokyo, Tokyo 113-0032, Japan

Submitted May 31, 2006; Revised October 16, 2006; Accepted October 19, 2006
Monitoring Editor: Martin A. Schwartz

We studied the spatiotemporal regulation of Akt (also called protein kinase B), phosphatidylinositol-3,4-bisphosphate [PtdIns(3,4)P_2], and phosphatidylinositol-3,4,5-trisphosphate [PtdIns(3,4,5)P_3] by using probes based on the principle of fluorescence resonance energy transfer. On epidermal growth factor (EGF) stimulation, the amount of PtdIns(3,4,5)P_3 was increased diffusely in the plasma membrane, whereas that of PtdIns(3,4)P_2 was increased more in the nascent lamellipodia than in the plasma membrane of the central region. The distribution and time course of Akt activation were similar to that of increased PtdIns(3,4)P_2 levels, which were most prominent in the nascent lamellipodia. Moreover, we found that upon EGF stimulation 3-phosphoinositide–dependent protein kinase-1 (PDK1) was also recruited to nascent lamellipodia in an Akt-dependent manner. Because PDK1 is known to activate Ral GTPase and because Ral is required for EGF-induced lamellipodial protrusion, we speculated that the PDK1–Akt complex may be indispensable for the induction of lamellipodia. In agreement with this idea, EGF-induced lamellipodia formation was promoted by the overexpression of Akt and inhibited by an Akt inhibitor or a Ral-binding domain of Sec5. These results identified the Akt–PDK1 complex as an upstream positive regulator of Ral GTPase in the induction of lamellipodial protrusion.

INTRODUCTION

Class I phosphoinositide 3-kinase (PI3K) is a key mediator of intracellular signaling pathways that regulate actin cytoskeletal reorganization and polarized cell migration. Activated PI3K phosphorylates phosphatidylinositol-4,5-bisphosphate [PtdIns(4,5)P_2] to generate phosphatidylinositol-3,4,5-trisphosphate [PtdIns(3,4,5)P_3], which, in turn, activates a variety of pleckstrin homology (PH) domain-containing proteins such as Akt (also called protein kinase B) (Saltiel and Pessin, 2002; Sulis and Parsons, 2003). PtdIns(3,4,5)P_3 is dephosphorylated to yield PtdIns(4,5)P_2 by a tumor suppressor protein, phosphatase and tensin homolog deleted in chromosome 10 (PTEN), which is frequently mutated or deleted in various human cancers (Sulis and Parsons, 2003). The resulting PTEN deficiency causes accumulation of PtdIns(3,4,5)P_3 in cells, and, as a consequence, an increase in cell motility in fibroblasts (Liliental *et al.*, 2000; Higuchi *et al.*, 2001; Hafizi *et al.*, 2005). Another dephosphorylated derivative of PtdIns (3,4,5)P_3 is PtdIns(3,4)P_2 produced by phosphoinositide 5-phosphatases, including Src homology 2-containing inositol-5-phosphatase (SHIP). This PtdIns(3,4)P_2 also binds to various PH domain-containing proteins, which overlap significantly to those bound to PtdIns(3,4,5)P_3 (Lemmon and Ferguson, 2000; Maffucci and Falasca, 2001).

Among many PH domain-containing proteins, a serine-threonine kinase, Akt, has been studied most extensively. Akt has been implicated in the control of diverse cellular functions, including glucose metabolism, gene transcription, cell proliferation, and apoptosis (Brazil *et al.*, 2004; Fayard *et al.*, 2005). Structurally, Akt is composed of three functionally distinct regions: an N-terminal PH domain that provides a lipid-binding module to direct Akt to PtdIns(3,4)P_2 and PtdIns(3,4,5)P_3, a central catalytic domain, and a C-terminal hydrophobic motif (Brazil *et al.*, 2004). Activation of Akt occurs when growth factors bind to receptor tyrosine kinases and activate PI3K, resulting in an increase in PtdIns(3,4,5)P_3 at the plasma membrane. The binding of PtdIns(3,4,5)P_3 to the PH domain anchors Akt to the plasma membrane and allows its phosphorylation and activation by 3-phosphoinositide–dependent protein kinase-1 (PDK1), another PH domain-containing protein. PDK1 phosphorylates Akt at Thr^{308}, which causes a charge-induced conformational change, allowing Akt for substrate binding and an increased rate of catalysis. Akt is further activated by the phosphorylation of Ser^{473}, which can be catalyzed by various kinases, including PDK2, DNA-PK, mammalian target of rapamysin, rictor complex, integrin linked kinase, and protein kinase CβII (Feng *et al.*, 2004; Kawakami *et al.*, 2004; Fayard *et al.*, 2005; Sarbassov *et al.*, 2005).

This article was published online ahead of print in *MBC in Press* (http://www.molbiolcell.org/cgi/doi/10.1091/mbc.E06-05-0467) on November 1, 2006.

The online version of this article contains supplemental material at *MBC Online* (http://www.molbiolcell.org).

Address correspondence to: Michiyuki Matsuda (matsudam@path1.med.kyoto-u.ac.jp).

It has been demonstrated that PI3K plays an essential role in the epidermal growth factor (EGF)-induced membrane protrusion by regulating not only Akt (Higuchi *et al.*, 2001; Nishita *et al.*, 2004; Hafizi *et al.*, 2005) but also Rac and Ral GTPases (Tian *et al.*, 2002; Gavard *et al.*, 2004; Nishita *et al.*, 2004; Takaya *et al.*, 2004). However, the mechanism by which Akt regulates the cytoskeletal remodeling and the relationship to Ral and Rac has been still remains elusive.

Ral GTPase has been shown to regulate exocytosis, endocytosis, and the actin cytoskeleton (for reviews, see Bos, 1998; Feig, 2003). Furthermore, essential roles for Ral have been demonstrated in cell migration (Suzuki *et al.*, 2000; Takaya *et al.*, 2004; Oxford *et al.*, 2005; Rosse *et al.*, 2006), and, more locally, in the induction of lamellipodial protrusion at the front of migrating cells (Takaya *et al.*, 2004). We have shown that PI3K, Cdc42, and Rac play important role in such localized activation of Ral (Takaya *et al.*, 2004). However, the mechanism by which spatial regulation of Ral activity is achieved is unknown.

Ral GTPase activity is regulated positively by Ral guanine nucleotide exchange factors (Ral GEFs) and negatively by GTPase-activating protein(s) (Feig *et al.*, 1996; Camonis and White, 2005). Three Ral GEFs, RalGDS, Rgl, and Rlf/Rgl2, are activated by Ras (Bos, 1998). However, Ral may be also activated by calcium signaling pathways (Hofer *et al.*, 1998). In C2C12 myoblasts and some other cell types, growth factors activate Ral in a manner dependent not only on Ras but also on calcium or PI3K signaling pathway (Suzuki *et al.*, 2000; Tian *et al.*, 2002; Takaya *et al.*, 2004). In contrast to GEFs, our knowledge of GAP is extremely limited and to date, proteins exhibiting Ral GAP activity are yet to be identified.

To understand the involvement of these signaling molecules in actin cytoskeleton reorganization, their spatiotemporal regulation has to be determined in living cells. To this end, in vivo probes have been developed based on the principle of fluorescence resonance energy transfer (FRET) (Zhang *et al.*, 2002; Jares-Erijman and Jovin, 2003). FRET is a nonradiative transfer of energy between two fluophores that are placed in proximity and in a proper relative angular orientation (Zhang *et al.*, 2002). Variants of green fluorescent protein (GFP) have provided genetically encoded fluophores that serve as donor and/or acceptor in FRET (Heim and Tsien, 1996; Mizuno *et al.*, 2001). Using these GFP variants and FRET technology, we previously developed genetically encoded probes for low-molecular-weight GTPases (Mochizuki *et al.*, 2001; Itoh *et al.*, 2005). Here, we introduce two FRET probes for the monitoring of Akt activity and the concentration of PtdIns(3,4,5)P_3 and PtdIns(3,4)P_2. With these newly developed FRET-based probes, we demonstrate that activation of Akt correlates more with the accumulation of PtdIns(3,4)P_2 than PtdIns(3,4,5)P_3. Furthermore, we have found that Akt forms a complex with PDK1 on the nascent lamellipodia, which leads to Ral activation.

MATERIALS AND METHODS

FRET Probes

Plasmids for FRET-based monitors were constructed essentially as described previously (Mochizuki *et al.*, 2001; Sato *et al.*, 2003). Akt Indicator (Akind) consisted of PH domain of Akt (a.a. 1-144), a spacer (Phe-Gly), yellow fluorescent protein (YFP), a spacer (Leu-Asp), catalytic domain of Akt (a.a. 133-480), a spacer (Gly-Gly-Arg), and cyan fluorescent protein (CFP). A FRET probe for PtdIns(3,4)P2, Pippi-PI(3,4)P_2, consisted of CFP, a spacer (Glu-Ala-Ala-Ala-Arg-Asp), PH domain of TAPP1 (a.a. 175-300), a spacer (Glu-Ala-Ala-Ala-Arg-Asp-Gly-Gly-Glu-Ala-Ala-Ala-Arg-Asp), YFP (a.a. 1-237), a spacer (Glu-Ala-Ala-Ala-Arg-Asp), and the CAAX box of Ki-Ras4B (a.a. 169-188). Other FRET probes, Raichu-Ras, Raichu-RalA, and Pippi-PI(3,4,5)P_3, have been described previously (Mochizuki *et al.*, 2001; Sato *et al.*, 2003; Takaya *et al.*, 2004; Aoki *et al.*, 2005).

Plasmids

cDNAs of Akt, Akt3A, and mDPH-Akt were subcloned into pERedNES, pCAGGS-Flag-C-mCFP, and/or pCAGGS-C-mVenus: pERedNES is for the internal ribosomal entry site-mediated expression of red fluorescent protein (RFP) with the nuclear export signal, allowing identification of the transfected cells under fluorescence microscope. pCAGGS-Flag-mCFP and pCAGGS-Flag-mVenus are expression vectors encoding a monomeric CFP and monomeric Venus, a YFP variant, respectively (Nagai *et al.*, 2002). cDNA of PDK1 was obtained from Alex Toker (Harvard Medical School, Boston, MA) and subcloned into pCXN2-mCFP, pCXN2-mVenus, pCXN2-HA, and pERedNLS. pERedNLS is similar to pERedNES except that RFP is tagged with nuclear localization signal (Yoshizaki *et al.*, 2004). pCXN2 vector is derived from pCAGGS and carries a neomycin resistance gene. cDNA of RalGDS was obtained from A. Wittinghofer (Max-Planck-Institut für Molekulare Physiologie, Dortmund, Germany) and subcloned into pCXN2–5myc vector. cDNA of Sec5 was obtained from Y. Ohta (Harvard Medical School). A DNA fragment of Sec5 (a.a. 1-99) was polymerase chain reaction (PCR) amplified and subcloned into pGEX-4T3.

Cell Culture, Transfection, and Immunoblotting

NIH 3T3 cells were purchased from the RIKEN Gene Bank (Wako-shi, Japan). Cos7 cells used in this study were Cos7/E3, a subclone of Cos7 cells established by Y. Fukui (Department of Applied Biological Chemistry, Graduate School of Agricultural and Life Sciences, University of Tokyo, Tokyo, Japan). NIH 3T3 and Cos7 cells were maintained in DMEM (Sigma-Aldrich, St. Louis, MO) supplemented with 10% fetal calf serum. For transient expression studies, cells were transfected using Polyfect (QIAGEN, Valencia, CA). Cells were analyzed at 24 h after transfection. Mock transfection was performed using the empty pCAGGS expression vector. For immunoblotting, proteins were separated by SDS-PAGE and transferred to a polyvinylidene difluoride membrane, followed by detection with antibodies described below. The bound antibodies were detected by an enhanced chemiluminescence (ECL) detection system (GE Healthcare, Little Chalfont, Buckinghamhsire, United Kingdom) and binding was quantified with the aid of an LAS-1000 image analyzer (Fuji-Film, Tokyo, Japan). Anti-GFP rabbit serum was prepared in our laboratory. Anti-RalA antibody was purchased from BD Biosciences (San Jose, CA). Anti-FLAG M2 antibody was purchased from Sigma-Aldrich. Anti-Myc 9E10 antibody was purchased from Santa Cruz Biotechnology (Santa Cruz, CA). Anti-GFP antibody was purchased from Takara Bio (Otsu, Japan). Anti-phosphoglycogen synthase kinase (GSK)3β (Ser21/9), Anti-PDK1, anti-Akt, and anti-phospho Akt (Thr^{308}) antibodies were purchased from Cell Signaling Technology (Beverly, MA). Akt inhibitor IV and LY294002 were purchased from Calbiochem (San Diego, CA).

Akt Kinase Assay

Akind-expressing cells were lysed for 10 min on ice in lysis buffer (20 mM Tris, pH 7.5, 150 mM NaCl, 1 mM EDTA, 1 mM EGTA, 1% Triton, 2.5 mM sodium pyrophosphate, 1 mM β-glycerophosphate, 1 mM Na_3VO_4, 1 μM phenylmethylsulfonyl fluoride [PMSF], 10 μg/ml leupeptin, and 10 μg/ml aprotinin). Akind was immunoprecipitated with high-affinity rat monoclonal anti-(hemagglutinin [HA]) A antibody (Roche Diagnostics, Indianapolis, IN) for 1 h at 4°C on protein A-Sepharose beads. Immunoprecipitates of Akind were washed twice with the lysis buffer and twice with the kinase buffer (25 mM Tris-HCl, pH 7.5, 5 mM β-glycerophosphate, 2 mM dithiothreitol, 0.1 mM Na_3VO_4, and 10 mM $MgCl_2$). Akind on beads was incubated for 30 min at 30°C in 40 μl of kinase buffer supplemented with 200 μM ATP and 1 μg of GSK3 fusion protein (Cell Signaling Technology). The GSK3 proteins were separated by SDS-PAGE followed by immunoblotting with anti-phospho-GSK Ser21/9 antibodies. Bound antibodies were detected by an ECL chemiluminescence detection system (GE Healthcare).

Coimmunoprecipitation Analysis among Akt, PDK1, and RalGDS

Akt-, HA-PDK1–, and Myc-RalGDS–expressing cells were lysed in lysis buffer (10 mM Tris-HCl, pH 7.5, 150 mM NaCl, 1 mM EDTA, 1% NP-40, 0.1% SDS, 1 mM Na_3VO_4, 1 μM PMSF, and 10 μg/ml aprotinin) and clarified by centrifugation. The supernatant was incubated with anti-anti-(HA A) antibody, anti c-Myc antibody (Sigma-Aldrich), or anti-Akt antibody (Cell Signaling Technology) for 30 min at 4°C. The lysate were incubated with protein A-Sepharose beads (GE Healthcare) for 1 h at 4°C, and the bound proteins and cell lysates were separated by SDS-PAGE, followed by immunoblotting with anti-anti-(HA A) antibody, anti-c-Myc antibody, or anti Akt antibody. Bound antibodies were detected by an ECL chemiluminescence detection system (GE Healthcare) and quantified with an LAS-1000 image analyzer (Fuji-Film).

Detection of RalA-GTP by Bos' Pull-Down Assay

Bos' pull-down assay for Ral proteins was performed essentially as described previously (Wolthuis *et al.*, 1998; Takaya *et al.*, 2004). Briefly, cells were lysed in Ral buffer (50 mM Tris-HCl, pH 7.5, 200 mM NaCl, 2.5 mM $MgCl_2$, 1% NP-40, 10% glycerol, 1 mM Na_3VO_4, 1 mM phenylmethylsulfunyl fluoride, 10 μg/ml aprotinin, and 10 μg/ml leupeptin) and clarified by centrifugation. The supernatant was incubated with GST-Sec5-RBD fusion proteins for 30 min at 4°C. The resulting complexes of Ral-GTP and GST-Sec5-RBD were incubated with glutathione-Sepharose beads (GE Healthcare) for 1 h at 4°C, and the bound proteins and cell lysates were separated by SDS-PAGE, followed by immunoblotting with anti-RalA antibodies. Bound antibodies were detected by an ECL chemiluminescence detection system (GE Healthcare) and quantified with an LAS-1000 image analyzer (Fuji-Film).

FRET Imaging

FRET imaging was performed essentially as described previously (Yoshizaki *et al.*, 2003). Briefly, cells plated on a collagen-coated 35-mm-diameter glass-base dish (Asahi Techno Glass, Tokyo, Japan) were imaged every 1 min on an Olympus IX81 inverted microscope (Olympus Optical, Tokyo, Japan) equipped with a laser-based autofocusing system, IX2-ZDC, and an automatically programmable XY stage, MD-XY30100T-Meta, which allowed us to obtain the time-lapse images of several view fields in a single experiment. For dual-emission ratio imaging of the intramolecular FRET probes, we used previously described filter sets and we obtained images for CFP and FRET. After background subtraction was carried out, the FRET/CFP ratio was depicted using MetaMorph software (Molecular Devices, Sunnyvale, CA), and this image was used to represent FRET efficiency. Filters used for the dual-emission ratio imaging were purchased from Omega Optical (Brattleboro, VT): an XF1071 (440AF21) excitation filter, an XF2034 (455DRLP) dichroic mirror, and two emission filters, XF3075 (480AF30) for CFP and XF3079 (535AF26) for FRET. Cells were illuminated with a 75-W xenon lamp through a 6% ND filter (Olympus Optical) and a 60× oil immersion objective lens. The exposure time was 0.3 s when the binning of the charge-coupled device (CCD) camera was set to 4 × 4. The ratio image of FRET/CFP was created with MetaMorph software and was used to represent the efficiency of the FRET.

Imaging with a pair of intermolecular FRET probes has been described previously (Sorkin *et al.*, 2000). Briefly, cells expressing a pair of proteins tagged with YFP and CFP, respectively, were imaged with the fluorescence microscope as described above except that an MX510 excitation filter (Asahi Spectra, Tokyo, Japan) and a 575ALP emission filter (Omega Optical) were used for the acquisition of YFP images and a semitransparent glass was used as a dichroic mirror throughout the imaging. Exposure times were 300 ms for CFP and FRET images and 300 ms for YFP images. Fluorescence through the FRET filter set consisted of a FRET component ("corrected" FRET, FRET) and non-FRET components, spectral bleedthrough and cross-excitation. The non-FRET components were subtracted as described previously (Sorkin *et al.*, 2000). For our experimental conditions, we used the following equation: cFRET = FRET − 0.37 × CFP − 0.71 × YFP.

Confocal FRET images were obtained by an IX51 upright fluorescence microscope (Olympus Optical) equipped with an intensified CCD camera (Hamamatsu Photonics, Hamamatsu, Japan), a CSU-10 spinning Nipkow disk confocal unit (Yokogawa Electric, Tokyo, Japan), a W-view emission image splitter (Hamamatsu Photonics), and a diode-pumped solid state 430-nm laser (Melles Griot, Carlsbad, CA).

RNA Interference

pSuper.retro.puro vector was used for short hairpin RNA (shRNA). The shRNA sequences for PTEN, SHIP2, and luciferase were 5′-GGATGGATTCGACTTAGAC-3′, 5′-GAATTATCTGGACATCCTG-3′, and 5′-GATTATGTCCGGTTATGTA-3′. NIH3T3 cells were transfected with the desired pSUPER constructs by using Lipofectamine 2000 (Invitrogen, Carlsbad, CA). After recovery, the cells were selected by 2-d incubation with 4 μg/ml puromycin and then used for further analysis.

Quantification of Growth Factor-induced Plasma Membrane Protrusion

Monomeric RFP-expressing Cos7 cells were time-lapse imaged every 2 min. The cell area 10 min after stimulation was divided by the cell area before stimulation to quantify the growth factor-induced membrane protrusion.

RESULTS

Development of an Akt Indicator, Akind

To investigate the spatiotemporal regulation of Akt, we developed a series of FRET probes for use in live cell imaging of Akt activity. For the sake of brevity, only the results obtained with the probe named Akind is described, because this probe performed best among those tested. From the amino terminus, Akind is composed of PH domain of Akt, YFP, catalytic and regulatory domains of Akt, and CFP from the amino terminus (Figure 1A). In this probe design, FRET level is low in the cytosolic inactive state and high in the membrane-recruited active state. We confirmed that Akind was regulated similarly to the endogenous Akt by showing that phosphorylation of Thr^{308} and in vitro kinase activity of Akind were increased upon stimulation by platelet-derived growth factor (PDGF) as efficiently as those of the endogenous Akt (Figure 1, B and C).

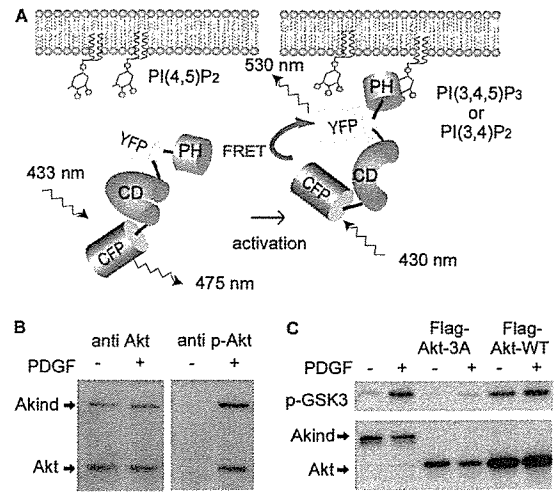

Figure 1. Development of a FRET probe for Akt. (A) Schematic representation of Akt Indicator (Akind). YFP and CFP denote a yellow-emitting mutant of GFP and cyan-emitting mutant of GFP, respectively. PH and CD indicate the pleckstrin homology domain and the catalytic domain of Akt, respectively. In this probe design, the FRET level increases when the probe is activated on the plasma membrane. (B) Akind-transfected NIH3T3 cells were analyzed by Western blotting with anti-Akt or anti-phospho-Thr^{308} of Akt before and after PDGF stimulation. (C) Akind-HA, Flag-Akt-WT, and Flag-Akt-3A expressed in PDGF-stimulated or nonstimulated NIH3T3 cells were immunoprecipitated with an anti-HA antibody or anti-FLAG antibody. Kinase activity was measured by using recombinant GSK3 as a substrate, of which phosphorylation was detected with anti-phospho-GSK3 antibody. A small aliquot of the immunoprecipitates were also analyzed with anti-FLAG antibody.

With this Akind probe, the activity change of Akt was time-lapse imaged in living NIH3T3 cells stimulated with PDGF (Figure 2A and Supplemental Video 1). As an index for Akt activation, we used the FRET/CFP value, which correlates with the proportion of Akind adopting active conformation at each pixel. On PDGF stimulation, transient accumulation of Akind and an increase in the FRET level were observed at the periphery of the cells, indicating the translocation and activation of Akt to the plasma membrane. A strong correlation between the Thr^{308} phosphorylation of endogenous Akt and FRET level was observed when the averaged FRET/CFP values in Akind-expressing NIH3T3 cells (n = 12) were plotted against time (Figure 2A). Similarly, we observed excellent correlation between Thr^{308} phosphorylation and FRET level in Cos7 cells stimulated with either insulin (n = 8) or EGF (n = 24), where the Akt activation prolonged in comparison with PDGF-stimulated NIH3T3 cells (Figure 2, B and C, and Supplemental Video 2). The strong correlation between the biochemical data obtained from bulk of cells and imaging data obtained from single cells clearly demonstrated that Akt behaves as an analog, but not digital, switch even in the single cell level. It is also important to note that the maximum increase in FRET

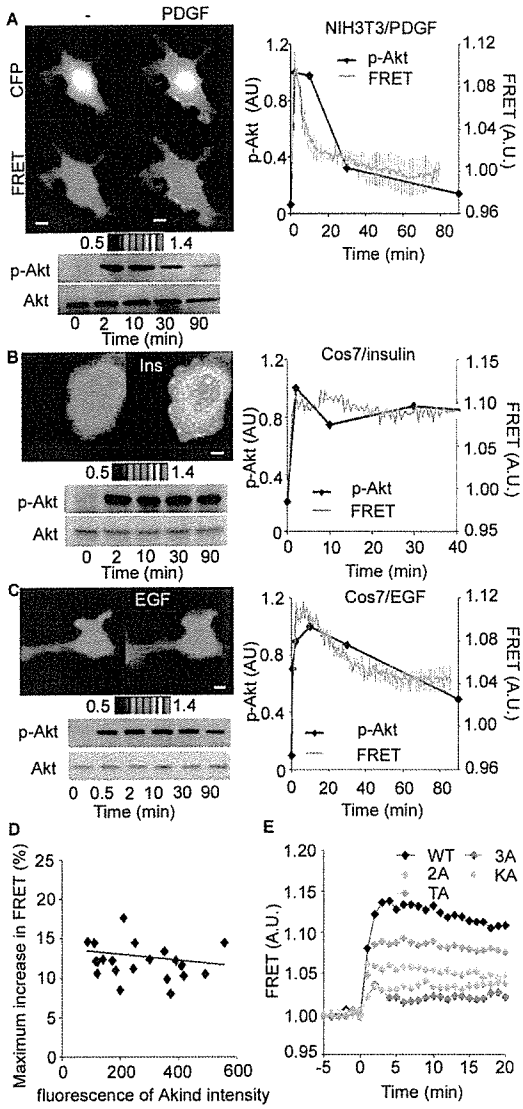

Figure 2. Akt activation in the nascent lamellipodia as monitored by Akind. (A) Akind-expressing NIH3T3 cells were serum starved for 24 h and stimulated with 50 ng/ml PDGF. CFP (excitation [ex] 440 nm/emission [em] 480 nm) and sensitized FRET (ex 440 nm/em 530 nm) images were obtained every 1 min with a time-lapse epifluorescent microscope. Ratio image of FRET/CFP was prepared to demonstrate the level of FRET (also available as Supplemental Video 1). At least 20 similar images were obtained. In the right panel, the net intensities of CFP and FRET in each cell were measured to calculate the averaged emission ratio (FRET/CFP). Then, the emission ratio values were normalized to those of the record-starting time. Data from more than 10 independent cells are shown with SE. Phosphorylation of endogenous Akt was also examined by immunoblotting and quantitated values are overlaid to the graph. Similar experiments were performed by using EGF-stimulated Cos7 cells (B and Supplemental video 2) and insulin-stimulated Cos7 cells (C). (D) Cell images used in B were used to negate the correlation between the FRET level at the zenith and the concentration of the probe. (E) Cos7 cells expressing Akt wild type or mutant (3A, 2A, KA, and TA) were serum starved for 24 h and stimulated with 50 ng/ml EGF as described in D. Bars, 10 μm.

level was not affected by the expression level of Akind (Figure 2D).

To understand the mechanism underlying the change in FRET efficiency, we prepared various Akind mutants with

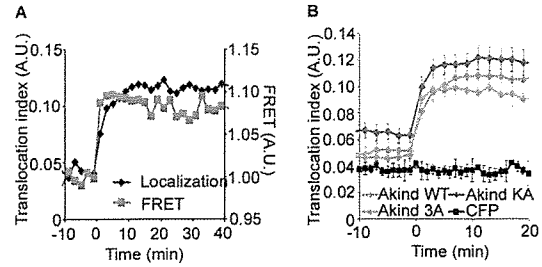

Figure 3. Semiquantitative analysis of plasma membrane translocation of Akind. Signal-dependent translocation of CFP-tagged cytosolic proteins to the plasma membrane was measured semiquantitatively by using RFP as a reference (for details, see Supplemental Material). (A) The translocation index and the FRET level of Cos7 cells expressing Akind were plotted against time. (B) Shown are time courses of the translocation index of cells expressing wild type, KA mutant, and 3A mutant of Akind.

impaired kinase activity by substituting alanine for the two major regulatory phosphorylation sites, Thr^{308} and Ser^{473}, or for the phosphate transfer residue in the catalytic site: TA, Thr308Ala; 2A, Thr308Ala and Ser473Ala; KA, Lys179Ala; 3A, all three mutations (Aoki *et al.*, 1998). Cos7 cells expressing these Akind mutants were stimulated with EGF and time-lapse imaged (Figure 2E). The maximum increase in the level of FRET showed an excellent correlation with the reported levels of the kinase activity of mutants: high in TA and low in 3A and KA mutants. Thus, we concluded that the activity-dependent conformational change of Akt could be monitored by the level of FRET in Akind-expressing cells.

We next examined the effect of the plasma membrane translocation of Akind on the FRET level. For this purpose, we established a semiquantitative assay for the plasma membrane translocation, which gives a translocation index as described in the Supplemental Material. With this assay, we quantitated the EGF-induced translocation of Akind to the plasma membrane and found that the increase in the translocation index correlated nicely with the increase in FRET level, indicating that the translocation and conformational change of Akt occurred almost simultaneously (Figure 3A). Importantly, however, both Akind-KA and Akind-3A mutants were found to translocate to the plasma membrane as efficiently as did the wild type (Figure 3B). This observation demonstrated that the translocation alone was not sufficient for the induction of conformational change of Akind and strongly suggested that changes in the FRET level monitored the conformational change accompanying the increased kinase activity of Akind.

Development of PtdIns(3,4)P_2 Indicator Pippi-PI(3,4)P_2

PtdIns(3,4,5)P_3 and PtdIns(3,4)P_2 have been shown to recruit Akt to the plasma membrane, where Akt becomes phosphorylated at Thr^{308} and Ser^{473} and is thereby activated enzymatically (Alessi *et al.*, 1996; Fayard *et al.*, 2005). To determine which of these two phosphoinositides determine the distribution of active Akt, we developed FRET-based monitors for the two phospholipids essentially as described previously (Figure 4A) (Sato *et al.*, 2003). The probe for PtdIns(3,4,5)P_3 named Pippi-PI(3,4,5)P_3, has been already reported and the probe for PtdIns(3,4)P_2 named Pippi-PI(3,4)P_2 was prepared by the use of PH domain of TAPP1, which binds specifically to PtdIns(3,4)P_2 (Dowler *et al.*, 2000). Pippi-PI(3,4)P_2 was found to detect PDGF-induced transient increase in PtdIns(3,4)P_2 very nicely (Figure 4B). The increase in the level of FRET was markedly inhibited by

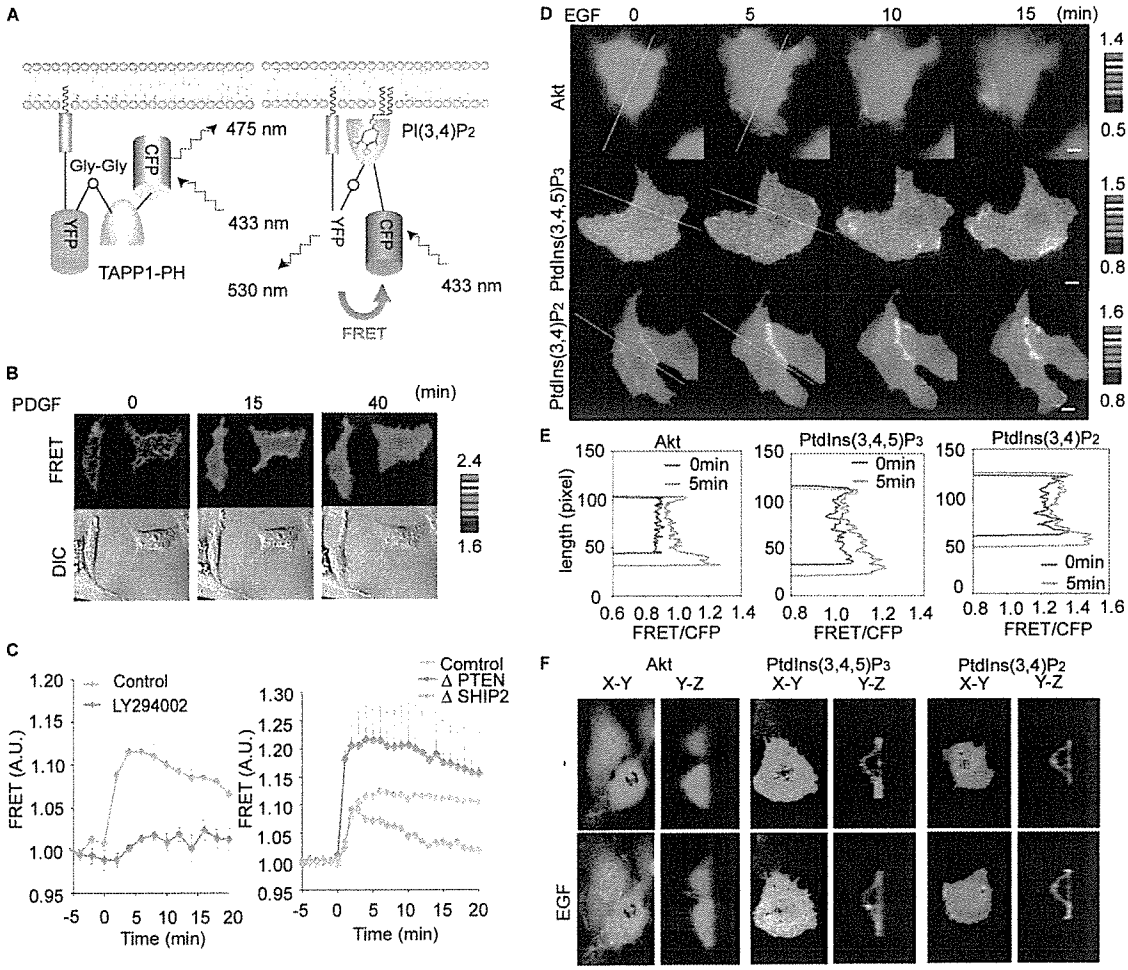

Figure 4. High Akt activity and accumulation of PtdIns(3,4)P_2 in the nascent lamellipodia. (A) Schematic representation of Pippi-PI(3,4)P_2. TAPP1-PH indicates the pleckstrin homology domain of TAPP1. The PH domain is sandwiched is by CFP and Venus. Venus and the PH domain are connected by means of rigid α-helical linkers consisting of repeated EAAAR sequences, between which is a single Gly-Gly motif introduced as a hinge. At the C terminus of Venus is the hypervariable region of K-Ras used as a plasma membrane-anchoring motif. Thus, the probes are designed to propagate high FRET signal when the PH domain binds to PtdIns(3,4)P_2. (B) NIH3T3 cells expressing Pippi-PI(3,4)P_2 were serum starved for 24 h and stimulated with 50 ng/ml PDGF. FRET imaging was performed as described in Figure 2. (C) Pippi-PI(3,4)P_2-expressing NIH3T3 cells untreated or treated with 40 μM LY294002 were stimulated with 50 ng/ml PDGF. The time course of the FRET level was obtained as in Figure 2. Cells were transfected with pSuper-PTEN, SHIP2, or luciferase, an shRNA vector, and selected by puromycin. Sixty hours posttransfection, FRET imaging was performed as described above. Averaged data from five cells are shown with SD. (D) Cos7 cells expressing Akind, Pippi-PI(3,4)P_2, or Pippi-PI(3,4,5)P_3 were serum starved for 24 h and stimulated with 50 ng/ml EGF. FRET images were obtained by a conventional epifluorescent microscope (D and Supplemental Videos 3 and 4). The FRET/CFP ratio image was used to show the FRET level in the intensity-modulated display mode. (E) Along the white lines in D, FRET/CFP values are plotted. (F) Cos7 cells prepared as described in D were imaged with a spinning disk confocal microscope. X-Y and Y-Z sections are shown. Bar, 10 μm.

LY294002 (Figure 4C, left). To further confirm the specificity of the Pippi-PI(3,4)P_2 probe, we examined the effect of knockdown of SHIP2 and PTEN (Figure 4C, right). PDGF-induced increase in PtdIns(3,4)P_2 was significantly enhanced in PTEN deficient cells, whereas the production of PtdIns (3,4)P_2 was suppressed in SHIP2-deficient cells. Intriguingly, the initial increase in PtdIns(3,4)P_2 was not impaired but the prolonged elevation was significantly suppressed in the SHIP2 knockdown cells.

Colocalization of High Akt Activity with Accumulation of PtdIns(3,4)P_2

With these two FRET probes, we monitored the dynamics of PtdIns(3,4)P_2 and PtdIns(3,4,5)P_3 in EGF-stimulated Cos7 cells (Figure 4D and Supplemental Videos 3 and 4). On EGF stimulation, the amount of PtdIns(3,4,5)P_3 was found to increase diffusely in the plasma membrane. This pattern of distribution was very similar to that of Ras and the EGF receptor (Mochizuki *et al.*, 2001; Itoh *et al.*, 2005). In contrast to PtdIns(3,4,5)P_3, PtdIns(3,4)P_2 concentration increased most prominently in the protruding lamellipodia and peripheral membrane ruffles. Line-scan plots of these FRET images emphasize the local accumulation of PtdIns(3,4)P_2 and activation of Akt (Figure 4E). Thus, the spatial distribution of Akt activation correlated more closely to the increase in PtdIns(3,4)P_2 rather than PtdIns(3,4,5)P_3. Because the apparent high FRET level in the cell periphery could be caused by the relatively small height of cell body, we confirmed our observation by spinning disk confocal microscopy (Figure 4F). An increase in PtdIns(3,4,5)P_3 was observed diffusely in the apical membrane. Increase in PtdIns(3,4)P_2 was also observed diffusely in the dorsal membrane; however, the

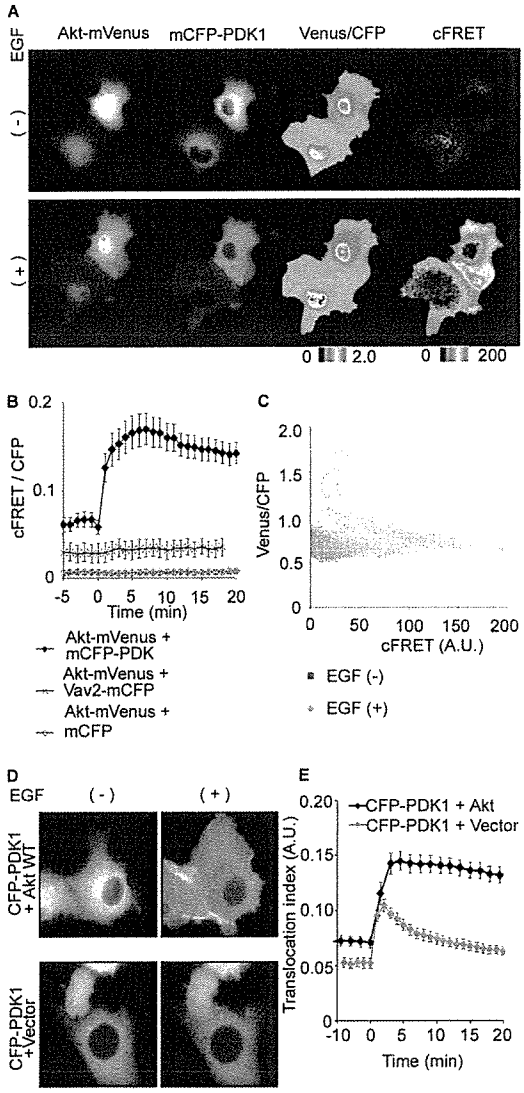

Figure 5. Accumulation of PDK1–Akt complex in nascent lamellipodia. (A and B) Cos7 cells expressing Akt-YFP and CFP-PDK1 were stimulated with 50 ng/ml EGF. Three images, CFP (ex 440 nm/em 480 nm), sensitized FRET (ex 440 nm/em 530 nm), and YFP (ex 510 nm/em 565 nm) were obtained every 30 s for 1 h. Corrected FRET (cFRET) images prepared as described in the text are shown in a pseudocolor mode (A). Net intensities of CFP and YFP in each cell were measured to calculate the averaged cFRET/CFP. (C) The Venus/CFP ratio values obtained from each pixel are plotted against cFRET. Pixels with YFP/CFP value over 1.0 corresponds those in the nucleus. (D) Cos7 cells expressing CFP-PDK1 in the presence or absence of Akt were stimulated with 50 ng/ml EGF and time-lapse imaged. (E) From each cell image, the translocation index of CFP-PDK1 were determined and plotted against time (n ≥ 18).

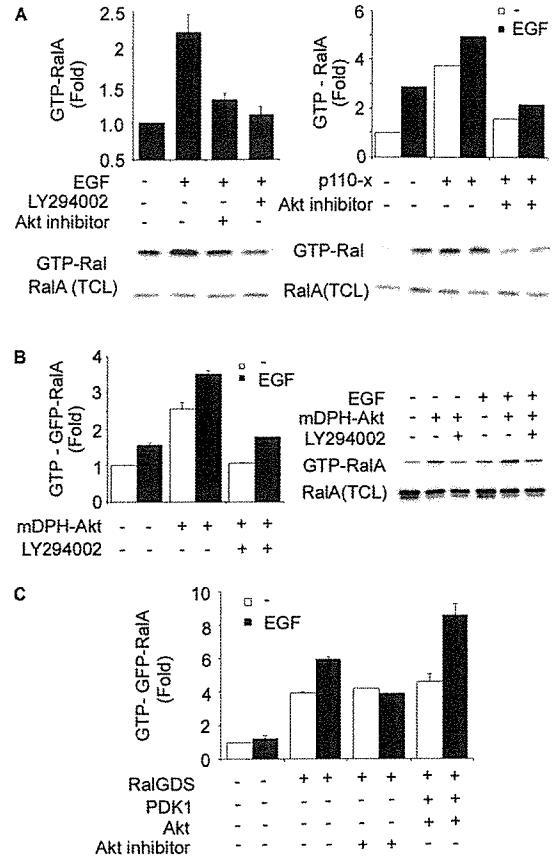

Figure 6. Requirement of Akt for EGF-induced RalA activation. (A) Cos7 cells transfected with or without an expression vector for a constitutively active mutant of PI3K, p110-x. Cells were serum starved for 8 h and left untreated or treated with LY294002 or Akt inhibitor IV for 30 min. The levels of endogenous GTP-Ral were assayed by Bos' pull-down method and quantitated with an LAS-1000 image analyzer. Averaged data from two independent experiments are shown with SE. (B) Cos7 cells transfected with or without an expression vector for GFP-RalA and a constitutively active mutant of Akt mDPH-Akt were serum starved for 8 h and left untreated or treated with LY294002. Cells with or without 50 ng/ml EGF stimulation were analyzed as described in A. (C) Cos7 cells expressing GFP-RalA with or without Myc-RalGDS were serum starved for 8 h and left untreated or treated with Aki inhibitor IV for 30 min before stimulation with 50 ng/ml EGF for 10 min. The level of GTP-bound GFP-RalA was analyzed as described in text.

increase was most prominent in the lamellipodia and peripheral membrane ruffles. The distribution of increased Akt activity was similar to that of PtdIns(3,4)P_2, i.e., most prominent in lamellipodia and the peripheral membrane ruffles. These results supported previous notes that Akt activation depends more on PtdIns(3,4)P_2 than PtdIns(3,4,5)P_3 (Franke *et al.*, 1997; Klippel *et al.*, 1997).

Accumulation of PDK1–Akt Complex at the Nascent Lamellipodial Protrusion

To further explore the mechanism of Akt activation in lamellipodia and peripheral membrane ruffles, we next investigated the role of PDK1, which is the major kinase that activates Akt at the plasma membrane. For this purpose, we prepared a pair of intermolecular FRET probes consisting of monomeric CFP-tagged PDK1 (mCFP-PDK1) and monomeric Venus-tagged Akt (Akt-mVenus). The intermolecular FRET level was then monitored in Cos7 cells expressing this pair of probes during EGF stimulation (Figure 5, A and B). We saw a significant increase in the FRET level in the peripheral region of cells, suggesting that the Akt–PDK1 complex was formed primarily at this location including lemellipodia. The distributions of Akt and PDK1 were similar except for nucleus and there were no significant correlation between Venus/CFP and cFRET values (Figure 5C). Thus, we could negate the possibility that the increase in FRET was caused by the accumulation of Akt-mVenus. When we used mCFP or mCFP-tagged Vav2, a PH domain-containing protein, as a FRET donor, the increase in FRET was not observed upon EGF stimulation (Figure 5B). Interestingly,

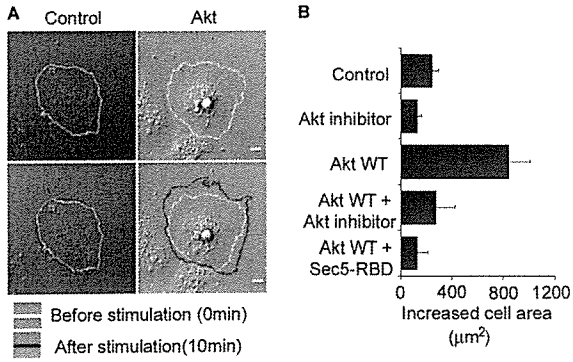

Figure 7. Requirement of Akt for EGF-induced membrane protrusion. (A) Parent and Akt-expressing Cos7 cells were stimulated with 50 ng/ml EGF. Differential interference contrast images of these cells were obtained every 1 min (top). White and black lines indicated the outlines of the cells before and 10 min after EGF stimulation, respectively. Bar, 10 μm. (B) Averaged extended cell areas, which was obtained by the reduction of black-lined area from white-lined area, are shown with SE (bottom). n ≥ 12.

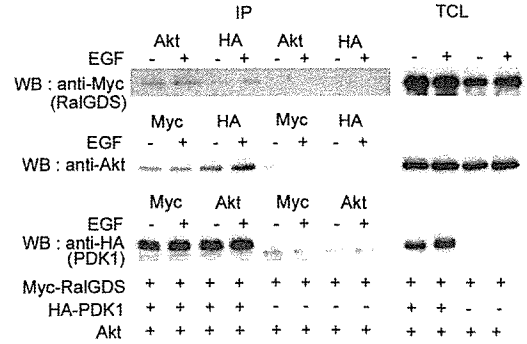

Figure 8. Association of Akt and RalGDS in a PDK1-dependent manner. Cos7 cells expressing Akt and Myc-RalGDS with or without HA-PDK1 were serum starved for 8 h and stimulated with 50 ng/ml EGF for 10 min. Cells were lysed and immunoprecipitated with anti-Myc monoclonal antibody (mAb), anti-HA rat mAb, or anti-Akt rabbit antibody. The immunoprecipitates (IP) and total cell lysates (TLC) were analyzed by immunoblotting.

we found that plasma membrane translocation of PDK1 was significantly enhanced and prolonged by the coexpression of Akt (Figure 5, D and E). Thus, the accumulation of the Akt–PDK complex at lamellipodial protrusion seemed to be caused primarily by Akt, which was recruited to the plasma membrane by PtdIns(3,4)P_2 and PtdIns(3,4,5)P_3.

Activation of RalGDS by PDK1–Akt Complex

We speculate that the accumulation of Akt–PDK1 complex at lamellipodia might induce Ral activation, based on the following two reasons. First, RalA activation is most prominent at nascent lamellipodia as is Akt activation (Figure 4D), and RalA activation is known to be dependent on PI3K (Tian *et al.*, 2002; Takaya *et al.*, 2004). Second, Feig and colleagues have reported that PDK1 serves as a scaffold to recruit and activate Ral GEFs at the plasma membrane (Tian *et al.*, 2002). In support of our model, we found that RalA activation by EGF or constitutively active mutant of PI3K was suppressed by the Akt inhibitor IV (Kau *et al.*, 2003) and that constitutively active Akt elevated the level of RalA-GTP (Figure 6, A and B). Furthermore, EGF-induced activation of RalA was enhanced by the coexpression of PDK1 and Akt (Figure 6C). Together, these data strongly suggests that Ral activation at the nascent lamellipodia is caused by Ral GEFs activated locally by the Akt–PDK1 complex.

Requirement of Akt Activity for EGF-induced Lamellipodia Protrusion

To demonstrate the Akt–PDK1 regulation of Ral in a physiological milieu, we examined the effect of the expression of Akt or Akt inhibitor IV on the EGF-induced lamellipodial protrusion, which has been shown to be dependent on Ral (Takaya *et al.*, 2004). The EGF-induced lamellipodia protrusion was significantly enhanced by the expression of Akt (Figure 7). This lamellipodial protrusion was markedly inhibited either by treatment with an Akt inhibitor IV or by the expression of the Ral binding domain of Sec5. Thus, our results identify the Akt–PDK complex at the cell periphery as an upstream positive regulator of Ral, which plays an essential role in the induction of lamellipodial protrusion.

Coimmunoprecipitation of Atk, PDK1, and RalGDS

To demonstrate the role of PDK1 in the formation of Akt–PDK1–RalGEF complex, we expressed Akt and RalGDS in the presence or absence of PDK1 and examined the complex formation (Figure 8). In the presence of PDK1, all three complexes of Akt-RalGDS, PDK1-RalGDS, and Akt-PDK1 were readily detected. In contrast, in the absence of PDK1, the Akt–RalGDS complex could not be detected, indicating that PDK1 functions as a scaffold to Akt and RalGDS (Figure 8).

DISCUSSION

Here, we propose that Akt stabilizes the PDK1–RalGEF complex at plasma membrane and thereby enhances Ral activation. The requirement of PI3K and PDK1 for Ral activation was originally reported by Tian *et al.* (2002). They have shown that PI3K-activated PDK1 binds to and activates RalGEF, resulting in Ral activation. In the same study, however, requirement of Akt was negated because kinase activity of PDK1 was dispensable for Ral activation and because Ral could not be activated by Akt-CAAX, an Akt mutant that contains the C-terminal CAAX motif of Ki-Ras and thereby localizes constitutively at the plasma membrane. However, in one study, it has been reported that this Akt-CAAX mutant lacks kinase activity and inhibits insulin-induced GSK3 activation by endogenous Akt (van Weeren *et al.*, 1998). Therefore, we used another active Akt mutant, mDPH-Akt, and found that this active Akt elevated basal and EGF-stimulated Ral activity (Figure 6). Conversely, treatment with Akt inhibitor IV decreased basal and EGF-stimulated Ral activity as did application of a PI3K inhibitor. Thus, by controlling the assembly of the PDK1–RalGEF complex, Akt serves as a critical determinant whether or not the molecular switch, Ral, should be turned on.

An important aspect of Akt regulation of Ral is in their spatial distribution. On EGF stimulation of Cos7 cells, RalGEF is recruited diffusely to the plasma membrane. Nevertheless, Ral activation is mostly observed at nascent lamellipodia, predicting the presence of another critical activator of Ral whose activity must have been elevated locally at the nascent lamellipodia (Takaya *et al.*, 2004). Akt meets the criteria of this spatial regulator of Ral. To further explore the mechanism underlying this Akt regulation of Ral activity, an Akt substrate that is phosphorylated in or close to the Akt–PDK1–RalGEF complex must be determined in the future study.

One major controversy concerning Akt activation is the issue of which PtdIns(3,4,5)P_3 and PtdIns(3,4)P_2 is the critical upstream regulator of Akt in vivo (Downward, 1998; Lemmon and Ferguson, 2000; Roymans and Slegers, 2001). There are substantial in vitro data suggesting that PtdIns(3,4)P_2 is more important than PtdIns(3,4,5)P_3 in Akt activation (Franke *et al.*, 1997; Frech *et al.*, 1997; Klippel *et al.*, 1997): Lipid vesicles containing PtdIns(3,4)P_2 activate Akt, whereas those containing PtdIns(3,4,5)P_3 either inhibit (Franke *et al.*, 1997; Frech *et al.*, 1997) or do not affect Akt activity (Klippel *et al.*, 1997). By using cells derived from SHIP-deficient mice, an essential role of PtdIns(3,4)P_2 has been demonstrated in Steel Factor-stimulated Akt activation (Scheid *et al.*, 2002). Our observations with FRET-based probes are in favor of this model: The increase in PtdIns(3,4)P_2 and activation of Akt were observed at the peripheral plasma membrane such as nascent lamellipodia, whereas an increase in PtdIns(3,4,5)P_3 was observed more diffusely at the plasma membrane, including the dorsal surface of the cells (Figure 4, D–F). On the contrary, in support of PtdIns(3,4,5)P_3 being the critical second messenger, PtdIns(3,4,5)P_3 is reported to bind to Akt with slightly higher affinity than does PtdIns(3,4)P_2 (James *et al.*, 1996; Frech *et al.*, 1997). Furthermore, PDK1 has a substantially higher affinity for PtdIns(3,4,5)P_3 than for PtdIns(3,4)P_2 (Stokoe *et al.*, 1997) and needs to interact with the plasma membrane to phosphorylate Akt efficiently (Anderson *et al.*, 1998). We also confirmed that the PH domain of PDK1 binds to PtdIns(3,4,5)P_3 more efficiently than to PtdIns(3,4)P_2 (data not shown). In vivo data in favor of PI(3,4,5)P_3 as the preferential regulator of Akt is obtained by using SHIP-overexpressing cells, where Akt activity is inhibited in the presence of high amount of PtdIns(3,4)P_2 (Aman *et al.*, 1998; Liu *et al.*, 1999; Taylor *et al.*, 2000).

In relation to this debate, we and others have observed that growth factor-induced membrane translocation of Akt is more readily detected than that of PDK1 (Figure 5D), although the affinity of the PH domain of PDK1 to PtdIns(3,4)P_2 and PtdIns(3,4,5)P_3 is higher than that of the PH domain of Akt (Currie *et al.*, 1999). This inefficient recruitment of PDK1 to the plasma membrane of growth factor-stimulated cells has been ascribed to the high-affinity binding of the PH domain of PDK1 to cytosolic Ins (1,3,4,5,6)P_5 and InsP_6 (Komander *et al.*, 2004). Considering these reports and data presented in the present study, it is likely that the plasma membrane recruitment of PDK1 is mediated partly by the PH domain-mediated interaction with PtdIns(3,4,5)P_3 and partly by the interaction with Akt and Ral GEF. In this context, the reason why the localization of Akt–PDK1 complex is similar to that of PtdIns(3,4)P_2, but not to that of PtdIns(3,4,5)P_3, should not be discussed based simply on the affinity of the PH domains to PtdIns(3,4)P_2 and PtdIns(3,4,5)P_3, but rather it should be considered in light of multiple factors that favors the production of PtdIns(3,4)P_2 and the formation of Akt–PDK1–Ral GEF complexes at localized areas of the plasma membrane, such as nascent lamellipodia.

Two types of FRET-based monitors of Akt activity have been reported previously (Calleja *et al.*, 2003; Sasaki *et al.*, 2003; Ananthanarayanan *et al.*, 2005; Kunkel *et al.*, 2005): 1) measurement of phosphorylation of Akt substrate (Sasaki *et al.*, 2003; Kunkel *et al.*, 2005) and 2) measurement of the conformational change of Akt (Calleja *et al.*, 2003). Probes belonging to the first type detect the balance between the activities of Akt and antagonizing phosphatases. For the acquisition of spatial information and high sensitivity, probes are preferentially anchored to the membrane, which may bias the interpretation of the results. Another restriction of this type of probe is in their sensitivity. Moreover, Ananthanarayanan *et al.* (2005) have observed a significant time-lag between the increase in the level of PtdIns(3,4,5)P_3 and activation of Akt monitored by a type 1 probe. The first probe belonging to the second type of probe was reported by Calleja *et al.* (2003). In this probe, designed for fluorescence lifetime imaging microscopy, GFP and YFP are fused to the amino and carboxy termini of Akt. We prepared a similar probe by using CFP and YFP as a FRET pair for ratiometry with a conventional epifluorescence microscope. However, this probe did not either translocate to plasma membrane or exhibit changes in the level of FRET in NIH3T3 cells (data not shown). This failure may be ascribable to the use of CFP as a FRET donor or subtle difference in the sequence of linker peptides. Thus, we tried several different designs of FRET monitors of Akt and reached to the structure of Akind. An advantage of Akind over type 1 probes is that both the activity and translocation of Akt can be monitored simultaneously and, indeed, we could for the first time visualize the accumulation and activation of Akt at the nascent lamellipodia (Figure 2). The precise mechanism of the FRET change upon Akt activation awaits further study. At least partly, phosphorylation-induced conformational change should be responsible because amino acid substitutions of phosphorylation sites diminished the level of FRET change upon activation (Figure 2).

In conclusion, the development of Akind has enabled us to visualize the localized activation of Akt, which led to the demonstration of the Akt–PDK1–Ral GEF complex at nascent lamellipodia. This finding seems to explain the reason why EGF-induced Ral activation is limited to the nascent lamellipodia.

ACKNOWLEDGMENTS

We thank Sam Yarwood for critical reading of this manuscript and S. Yoshiki, N. Fujimoto, and K. Fukuhara for technical assistance. This work was supported by a grant-in-aid for scientific research on priority areas entitled "Integrative Research Toward the Conquest of Cancer" from the Ministry of Education, Culture, Sports, Science, and Technology of Japan.

REFERENCES

Alessi, D. R., Andjelkovic, M., Caudwell, B., Cron, P., Morrice, N., Cohen, P., and Hemmings, B. A. (1996). Mechanism of activation of protein kinase B by insulin and IGF-1. EMBO J. *15*, 6541–6551.

Aman, M. J., Lamkin, T. D., Okada, H., Kurosaki, T., and Ravichandran, K. S. (1998). The inositol phosphatase SHIP inhibits Akt/PKB activation in B cells. J. Biol. Chem. *273*, 33922–33928.

Ananthanarayanan, B., Ni, Q., and Zhang, J. (2005). Signal propagation from membrane messengers to nuclear effectors revealed by reporters of phosphoinositide dynamics and Akt activity. Proc. Natl. Acad. Sci. USA *102*, 15081–15086.

Anderson, K. E., Coadwell, J., Stephens, L. R., and Hawkins, P. T. (1998). Translocation of PDK-1 to the plasma membrane is important in allowing PDK-1 to activate protein kinase B. Curr. Biol. *8*, 684–691.

Aoki, K., Nakamura, T., Fujikawa, K., and Matsuda, M. (2005). Local phosphatidylinositol 3,4,5-trisphosphate accumulation recruits Vav2 and Vav3 to activate Rac1/Cdc42 and initiate neurite outgrowth in nerve growth factor-stimulated PC12 cells. Mol. Biol. Cell *16*, 2207–2217.

Aoki, M., Batista, O., Bellacosa, A., Tsichlis, P., and Vogt, P. K. (1998). The akt kinase: molecular determinants of oncogenicity. Proc. Natl. Acad. Sci. USA *95*, 14950–14955.

Bos, J. L. (1998). All in the family? New insights and questions regarding interconnectivity of Ras, Rap1 and Ral. EMBO J. *17*, 6776–6782.

Brazil, D. P., Yang, Z. Z., and Hemmings, B. A. (2004). Advances in protein kinase B signalling: AKTion on multiple fronts. Trends Biochem. Sci. *29*, 233–242.

Calleja, V., Ameer-Beg, S. M., Vojnovic, B., Woscholski, R., Downward, J., and Larijani, B. (2003). Monitoring conformational changes of proteins in cells by fluorescence lifetime imaging microscopy. Biochem. J. *372*, 33–40.

Camonis, J. H., and White, M. A. (2005). Ral GTPases: corrupting the exocyst in cancer cells. Trends Cell Biol. *15*, 327–332.

Currie, R. A., Walker, K. S., Gray, A., Deak, M., Casamayor, A., Downes, C. P., Cohen, P., Alessi, D. R., and Lucocq, J. (1999). Role of phosphatidylinositol 3,4,5-trisphosphate in regulating the activity and localization of 3-phosphoinositide-dependent protein kinase-1. Biochem. J. *337*, 575–583.

Dowler, S., Currie, R. A., Campbell, D. G., Deak, M., Kular, G., Downes, C. P., and Alessi, D. R. (2000). Identification of pleckstrin-homology-domain-containing proteins with novel phosphoinositide-binding specificities. Biochem. J. *351*, 19–31.

Downward, J. (1998). Mechanisms and consequences of activation of protein kinase B/Akt. Curr. Opin. Cell Biol. *10*, 262–267.

Fayard, E., Tintignac, L. A., Baudry, A., and Hemmings, B. A. (2005). Protein kinase B/Akt at a glance. J. Cell Sci. *118*, 5675–5678.

Feig, L. A. (2003). Ral-GTPases: approaching their 15 minutes of fame. Trends Cell Biol. *13*, 419–425.

Feig, L. A., Urano, T., and Cantor, S. (1996). Evidence for a Ras/Ral signaling cascade. Trends Biochem. Sci. *21*, 438–441.

Feng, J., Park, J., Cron, P., Hess, D., and Hemmings, B. A. (2004). Identification of a PKB/Akt hydrophobic motif Ser-473 kinase as DNA-dependent protein kinase. J. Biol. Chem. *279*, 41189–41196.

Franke, T. F., Kaplan, D. R., Cantley, L. C., and Toker, A. (1997). Direct regulation of the Akt proto-oncogene product by phosphatidylinositol-3,4-bisphosphate. Science *275*, 665–668.

Frech, M., Andjelkovic, M., Ingley, E., Reddy, K. K., Falck, J. R., and Hemmings, B. A. (1997). High affinity binding of inositol phosphates and phosphoinositides to the pleckstrin homology domain of RAC/protein kinase B and their influence on kinase activity. J. Biol. Chem. *272*, 8474–8481.

Gavard, J., Lambert, M., Grosheva, I., Marthiens, V., Irinopoulou, T., Riou, J. F., Bershadsky, A., and Mege, R. M. (2004). Lamellipodium extension and cadherin adhesion: two cell responses to cadherin activation relying on distinct signalling pathways. J. Cell Sci. *117*, 257–270.

Hafizi, S., Ibraimi, F., and Dahlback, B. (2005). C1-TEN is a negative regulator of the Akt/PKB signal transduction pathway and inhibits cell survival, proliferation, and migration. FASEB J. *19*, 971–973.

Heim, R., and Tsien, R. Y. (1996). Engineering green fluorescent protein for improved brightness, longer wavelengths and fluorescence resonance energy transfer. Curr. Biol. *6*, 178–182.

Higuchi, M., Masuyama, N., Fukui, Y., Suzuki, A., and Gotoh, Y. (2001). Akt mediates Rac/Cdc42-regulated cell motility in growth factor-stimulated cells and in invasive PTEN knockout cells. Curr. Biol. *11*, 1958–1962.

Hofer, F., Berdeaux, R., and Martin, G. S. (1998). Ras-independent activation of Ral by a Ca(2+)-dependent pathway. Curr. Biol. *8*, 839–842.

Itoh, R. E., Kurokawa, K., Fujioka, A., Sharma, A., Mayer, B. J., and Matsuda, M. (2005). A FRET-based probe for epidermal growth factor receptor bound non-covalently to a pair of synthetic amphipathic helixes. Exp. Cell Res. *307*, 142–152.

James, S. R., Downes, C. P., Gigg, R., Grove, S. J., Holmes, A. B., and Alessi, D. R. (1996). Specific binding of the Akt-1 protein kinase to phosphatidylinositol 3,4,5-trisphosphate without subsequent activation. Biochem. J. *315*, 709–713.

Jares-Erijman, E. A., and Jovin, T. M. (2003). FRET imaging. Nat. Biotechnol. *21*, 1387–1395.

Kau, T. R., Schroeder, F., Ramaswamy, S., Wojciechowski, C. L., Zhao, J. J., Roberts, T. M., Clardy, J., Sellers, W. R., Silver, P. A. (2003). A chemical genetic screen identifies inhibitors of regulated nuclear export of a Forkhead transcription factor in PTEN-deficient tumor cells. Cancer Cell *4*, 463–476.

Kawakami, Y., Nishimoto, H., Kitaura, J., Maeda-Yamamoto, M., Kato, R. M., Littman, D. R., Leitges, M., Rawlings, D. J., and Kawakami, T. (2004). Protein kinase C betaII regulates Akt phosphorylation on Ser-473 in a cell type- and stimulus-specific fashion. J. Biol. Chem. *279*, 47720–47725.

Klippel, A., Kavanaugh, W. M., Pot, D., and Williams, L. T. (1997). A specific product of phosphatidylinositol 3-kinase directly activates the protein kinase Akt through its pleckstrin homology domain. Mol. Cell Biol. *17*, 338–344.

Komander, D., Fairservice, A., Deak, M., Kular, G. S., Prescott, A. R., Peter, D. C., Safrany, S. T., Alessi, D. R., and van Aalten, D. M. (2004). Structural insights into the regulation of PDK1 by phosphoinositides and inositol phosphates. EMBO J. *23*, 3918–3928.

Kunkel, M. T., Ni, Q., Tsien, R. Y., Zhang, J., and Newton, A. C. (2005). Spatio-temporal dynamics of protein kinase B/Akt signaling revealed by a genetically encoded fluorescent reporter. J. Biol. Chem. *280*, 5581–5587.

Lemmon, M. A., and Ferguson, K. M. (2000). Signal-dependent membrane targeting by pleckstrin homology (PH) domains. Biochem. J. *350*, 1–18.

Liliental, J., Moon, S. Y., Lesche, R., Mamillapalli, R., Li, D., Zheng, Y., Sun, H., and Wu, H. (2000). Genetic deletion of the Pten tumor suppressor gene promotes cell motility by activation of Rac1 and Cdc42 GTPases. Curr. Biol. *10*, 401–404.

Liu,Q., Sasaki, T., Kozieradzki, I., Wakeham, A., Itie, A., Dumont, D. J., and Penninger, J. M. (1999). SHIP is a negative regulator of growth factor receptor-mediated PKB/Akt activation and myeloid cell survival. Genes Dev. *13*, 786–791.

Maffucci, T., and Falasca, M. (2001). Specificity in pleckstrin homology (PH) domain membrane targeting: a role for a phosphoinositide-protein co-operative mechanism. FEBS Lett. *506*, 173–179.

Mizuno, H., Sawano, A., Eli, P., Hama, H., and Miyawaki, A. (2001). Red fluorescent protein from *Discosoma* as a fusion tag and a partner for fluorescence resonance energy transfer. Biochemistry *40*, 2502–2510.

Mochizuki, N., Yamashita, S., Kurokawa, K., Ohba, Y., Nagai, T., Miyawaki, A., and Matsuda, M. (2001). Spatio-temporal images of growth-factor-induced activation of Ras and Rap1. Nature *411*, 1065–1068.

Nagai, T., Ibata, K., Park, E. S., Kubota, M., Mikoshiba, K., and Miyawaki, A. (2002). A variant of yellow fluorescent protein with fast and efficient maturation for cell-biological applications. Nat. Biotechnol. *20*, 87–90.

Nishita, M., Wang, Y., Tomizawa, C., Suzuki, A., Niwa, R., Uemura, T., and Mizuno, K. (2004). Phosphoinositide 3-kinase-mediated activation of cofilin phosphatase Slingshot and its role for insulin-induced membrane protrusion. J. Biol. Chem. *279*, 7193–7198.

Oxford, G., Owens, C. R., Titus, B. J., Foreman, T. L., Herlevsen, M. C., Smith, S. C., and Theodorescu, D. (2005). RalA and RalB: antagonistic relatives in cancer cell migration. Cancer Res. *65*, 7111–7120.

Rosse, C., Hatzoglou, A., Parrini, M. C., White, M. A., Chavrier, P., and Camonis, J. (2006). RalB mobilizes the exocyst to drive cell migration. Mol. Cell Biol. *26*, 727–734.

Roymans, D., and Slegers, H. (2001). Phosphatidylinositol 3-kinases in tumor progression. Eur. J. Biochem. *268*, 487–498.

Saltiel, A. R., and Pessin, J. E. (2002). Insulin signaling pathways in time and space. Trends Cell Biol. *12*, 65–71.

Sarbassov, D. D., Guertin, D. A., Ali, S. M., and Sabatini, D. M. (2005). Phosphorylation and regulation of Akt/PKB by the rictor-mTOR complex. Science *307*, 1098–1101.

Sasaki, K., Sato, M., and Umezawa, Y. (2003). Fluorescent indicators for Akt/protein kinase B and dynamics of Akt activity visualized in living cells. J. Biol. Chem. *278*, 30945–30951.

Sato, M., Ueda, Y., Takagi, T., and Umezawa, Y. (2003). Production of PtdInsP3 at endomembranes is triggered by receptor endocytosis. Nat. Cell Biol. *5*, 1016–1022.

Scheid, M. P., Huber, M., Damen, J. E., Hughes, M., Kang, V., Neilsen, P., Prestwich, G. D., Krystal, G., and Duronio, V. (2002). Phosphatidylinositol (3,4,5)P3 is essential but not sufficient for protein kinase B (PKB) activation; phosphatidylinositol (3,4)P2 is required for PKB phosphorylation at Ser-473; studies using cells from SH2-containing inositol-5-phosphatase knockout mice. J. Biol. Chem. *277*, 9027–9035.

Sorkin, A., McClure, M., Huang, F., and Carter, R. (2000). Interaction of EGF receptor and grb2 in living cells visualized by fluorescence resonance energy transfer (FRET) microscopy. Curr. Biol. *10*, 1395–1398.

Stokoe, D., Stephens, L. R., Copeland, T., Gaffney, P. R., Reese, C. B., Painter, G. F., Holmes, A. B., McCormick, F., and Hawkins, P. T. (1997). Dual role of phosphatidylinositol-3,4,5-trisphosphate in the activation of protein kinase B. Science *277*, 567–570.

Sulis, M. L., and Parsons, R. (2003). PTEN: from pathology to biology. Trends Cell Biol. *13*, 478–483.

Suzuki, J., Yamazaki, Y., Li, G., Kaziro, Y., and Koide, H. (2000). Involvement of Ras and Ral in chemotactic migration of skeletal myoblasts. Mol. Cell Biol. *20*, 4658–4665.

Takaya, A., Ohba, Y., Kurokawa, K., and Matsuda, M. (2004). RalA activation at nascent lamellipodia of epidermal growth factor-stimulated Cos7 cells and migrating Madin-Darby canine kidney cells. Mol. Biol. Cell *15*, 2549–2557.

Taylor, V., Wong, M., Brandts, C., Reilly, L., Dean, N. M., Cowsert, L. M., Moodie, S., and Stokoe, D. (2000). 5′ phospholipid phosphatase SHIP-2 causes protein kinase B inactivation and cell cycle arrest in glioblastoma cells. Mol. Cell Biol. *20*, 6860–6871.

Tian, X., Rusanescu, G., Hou, W., Schaffhausen, B., and Feig, L. A. (2002). PDK1 mediates growth factor-induced Ral-GEF activation by a kinase-independent mechanism. EMBO J. *21*, 1327–1338.

van Weeren, P. C., de Bruyn, K. M., Vries-Smits, A. M., van Lint, J., and Burgering, B. M. (1998). Essential role for protein kinase B (PKB) in insulin-induced glycogen synthase kinase 3 inactivation. Characterization of dominant-negative mutant of PKB. J. Biol. Chem. *273*, 13150–13156.

Wolthuis, R. M., Franke, B., van Triest, M., Bauer, B., Cool, R. H., Camonis, J. H., Akkerman, J. W., and Bos, J. L. (1998). Activation of the small GTPase Ral in platelets. Mol. Cell Biol. *18*, 2486–2491.

Yoshizaki, H., Ohba, Y., Kurokawa, K., Itoh, R. E., Nakamura, T., Mochizuki, N., Nagashima, K., and Matsuda, M. (2003). Activity of Rho-family GTPases during cell division as visualized with FRET-based probes. J. Cell Biol. *162*, 223–232.

Yoshizaki, H., Ohba, Y., Parrini, M. C., Dulyaninova, N. G., Bresnick, A. R., Mochizuki, N., and Matsuda, M. (2004). Cell type-specific regulation of RhoA activity during cytokinesis. J. Biol. Chem. *279*, 44756–44762.

Zhang, J., Campbell, R. E., Ting, A. Y., and Tsien, R. Y. (2002). Creating new fluorescent probes for cell biology. Nat. Rev. Mol. Cell Biol. *3*, 906–918.

EXPERIMENTAL CELL RESEARCH 313 (2007) 698–706

available at www.sciencedirect.com

ScienceDirect

www.elsevier.com/locate/yexcr

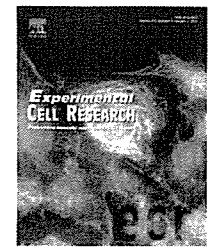

Research Article

Single-cell-derived mesenchymal stem cells overexpressing Csx/Nkx2.5 and GATA4 undergo the stochastic cardiomyogenic fate and behave like transient amplifying cells

Yoji Yamada[a], Kazuhiro Sakurada[a,1], Yukiji Takeda[b,2], Satoshi Gojo[b,3], Akihiro Umezawa[b,*]

[a]BioFrontier Laboratories, Kyowa Hakko Kogyo Co. Ltd., 3-6-6 Asahi-machi, Machida-shi, Tokyo 194-8533, Japan
[b]National Research Institute for Child Health and Development, 2-10-1 Okura, Setagaya-ku, Tokyo 157-8535, Japan

ARTICLE INFORMATION

Article Chronology:
Received 22 June 2006
Revised version received
31 October 2006
Accepted 15 November 2006
Available online 30 November 2006

Keywords:
Mesenchymal stem cells
Cardiomyocytes
Transient amplifying cells
Csx/Nkx2.5
GATA4

ABSTRACT

Bone marrow-derived stromal cells can give rise to cardiomyocytes as well as adipocytes, osteocytes, and chondrocytes in vitro. The existence of mesenchymal stem cells has been proposed, but it remains unclear if a single-cell-derived stem cell stochastically commits toward a cardiac lineage. By single-cell marking, we performed a follow-up study of individual cells during the differentiation of 9-15c mesenchymal stromal cells derived from bone marrow cells. Three types of cells, i.e., cardiac myoblasts, cardiac progenitors and multipotent stem cells were differentiated from a single cell, implying that cardiomyocytes are generated stochastically from a single-cell-derived stem cell. We also demonstrated that overexpression of Csx/Nkx2.5 and GATA4, precardiac mesodermal transcription factors, enhanced cardiomyogenic differentiation of 9-15c cells, and the frequency of cardiomyogenic differentiation was increased by co-culturing with fetal cardiomyocytes. Single-cell-derived mesenchymal stem cells overexpressing Csx/Nkx2.5 and GATA4 behaved like cardiac transient amplifying cells, and still retained their plasticity in vivo.

Introduction

Cell-based therapy is a novel therapeutic strategy, based on the concept of the cell-mediated restoration of damaged or diseased tissue. Candidate cell sources include embryonic stem (ES) cells, hematopoietic stem cells (HSCs), neural stem cells (NSCs), mesenchymal stem cells (MSCs) [1], and so on. Clinical trials with MSCs have been performed in patients with graft-versus-host disease through immunomodulatory effects [2], and osteogenesis imperfecta [3,4], and MSCs are expected to be one of the most available cells. The source of MSCs includes bone marrow [5], adipose tissue [6], umbilical cord [7] and placenta [8].

Bone marrow-derived stromal cells [9] can differentiate into mesenchymal progenitors, including osteoblasts [10], chondroblasts [11], skeletal myoblasts [12], adipoblasts [13],

* *Corresponding author.*
E-mail address: umezawa@1985.jukuin.keio.ac.jp (A. Umezawa).
[1] Present address: Research Center, Nihon Schering K.K., 1-5-5 Minatojima-minamicho, Chuo-ku, Kobe-shi, Hyogo 650-0047, Japan.
[2] Present address: Department of General Medicine and Clinical Investigation, Nara Medical University, 840 Shijo-cho, Kashihara-city, Nara 634-8522, Japan.
[3] Present address: Department of Cardiovascular Surgery, Saitama Medical Center, 1981 Kamoda, Kawagoe, Saitama 350-8550, Japan.

0014-4827/$ – see front matter © 2006 Elsevier Inc. All rights reserved.
doi:10.1016/j.yexcr.2006.11.012

and neurons [14,15] when placed in appropriate in vitro and in vivo environments. We have shown that bone marrow-derived stromal cells are also able to differentiate into cardiomyocytes in vitro and in vivo [13,14,16,17]. However, the characteristics of the cells that can differentiate into cardiomyocytes are poorly understood, and how the progeny of multipotent cells adopt one fate among several possible fates remains a fundamental question.

Hematopoietic stem cells are defined as cells that are capable of self-renewal to maintain a long-term supply of progeny and are capable of differentiating into multiple hematopoietic lineages [18]. Retroviral labeling of individual cells is one of the useful clonal assays to monitor lineage commitment at the single cell level [16,17,19]. At present, several models have been proposed in which hematopoietic lineage determination is driven intrinsically [20], extrinsically [21], or both [22]. We therefore performed retroviral labeling experiments of bone marrow-derived stromal cells to investigate whether cardiomyocytes are generated from committed cardiac precursor cells or uncommitted stem cells.

In the present study, we provide evidence that cardiomyocytes are stochastically differentiated from MSCs, and we demonstrate that forced expression of cardiomyocyte-specific transcription factors, i.e., Csx/Nkx2.5 and GATA4, destined these MSCs to a cardiomyocytic lineage.

Materials and methods

Cell culture

9-15c cells were used as a source of uncommitted stem cells in this study [23,24]. 9-15c cells are available through one of the cell banks (JHSF cell bank: http://www.jhsf.or.jp/English/index_gc.html; RIKEN cell bank: http://www.brc.riken.go.jp/lab/cell/english/guide.shtml). 9-15c cells were cultured using methods described previously [25]. The cells were cultured in Iscove's modified Dulbecco's medium (IMDM) supplemented with 20% fetal bovine serum and penicillin (100 μg/ml)/streptomycin (100 μg/ml)/amphotericin B (250 ng/ml) at 33°C with 5% CO_2.

Primary cultures of cardiac myocytes were prepared from the hearts of 16-day-old fetal C3H/HeJ mice (CLEA Japan, Inc., Tokyo, Japan) according to the method of Simpson et al. [26] with minor modifications. In brief, cardiomyocytes were dissociated into single isolated cells by trypsinization and the cells were plated in culture medium (IMDM with 20% fetal bovine serum).

Cloning of Csx/Nkx2.5 and GATA4 cDNAs

The full open reading frames of mouse Csx/Nkx2.5 and GATA4 cDNAs were cloned by RT-PCR from poly(A) RNA obtained from the hearts of fetal mice using the following primers: Csx/Nkx2.5, sense: 5′-TGAAACCTGCGTCGCCACCATGT-3′, antisense: 5′-GGCTCTTTCCCTACCAGGCTCGG-3′; GATA4, sense: 5′-TAGTTCTTGTCTGCCTCGTGCTCA-3′, antisense: 5′-GGCGCTGATTACGCGGTGATTATG-3′. The PCR products were subcloned into pGEM-T vector (Promega). DNA sequencing confirmed that the plasmids contained the full-length fragments of the mouse Csx/Nkx2.5 and GATA4 coding regions.

Retroviral transduction

The retroviral vectors pCLNCX (Imgenex), pCLPCX and pCLHCX were used. pCLPCX was constructed from pCLNCX by replacing the neomycin resistance gene with a puromycin resistance gene (pPUR; CLONTECH). pCLHCX was constructed from pCLNCX by replacing the neomycin resistance gene with a hygromycin resistance gene (pcDNA3.1/Hygro(+); Invitrogen). Fragments containing the EGFP, Csx/Nkx2.5, and GATA4 genes were cloned into pCLNCX, pCLPCX, or pCLHCX. Each of these DNAs and pCMV-Eco (kindly provided by Nikunj Somia) were transfected into the producer cells (293 gag pol; kindly provided by Nikunj Somia) using TransFast (Promega). Two days after the transfection, the culture supernatant was filtered through a 0.45-μm filter. 9-15c cells were treated with viruses and hexadimethine bromide (polybrene) (Sigma) (8 μg/ml) for 4–6 h. To generate stably expressing cells, 9-15c cells were cultured in the presence of 300 μg/ml G418, 300 ng/ml puromycin or 300 μg/ml hygromycin. The mixtures of drug-resistant clones were used to average the clonal variation of the transfected gene expression.

Cardiomyogenic induction

To induce differentiation, cells were initially plated at a density of 2×10^4 cells/ml. The cells were treated with 3 μM 5-azacytidine (Sigma) for 24 h the next day. In some experiments, PDGF-BB (Peprotech) and retinoic acid (Sigma) were added to the culture dish coated with fibronectin (BD Biosciences) to give a final concentration of 10 ng/ml and 1 nM, respectively, for 6 days. Total number of beating cells was estimated under phase contrast microscopy.

RT-PCR

Total RNA was extracted from adult mouse hearts, skeletal muscles and cultured cells with an RNeasy kit (QIAGEN), and cDNA was made using the SuperScript First-strand Synthesis System (Invitrogen) from 1 μg of total RNA. First-strand cDNA was diluted 20 fold and 1 μl of cDNA was used for each PCR reaction. The following primer sets for cardiomyocyte-associated genes were used: atrial natriuretic peptide (ANP), sense: 5′-TTCCTCGTCTTGGCCTTTTGG-3′, antisense: 5′-GCTGGATCTTCGTAGGCTCCG-3′; cardiac troponin I (cTnI), sense: 5′-GATCCTGTTCTCTGCCTCTGGA-3′, antisense: 5′-TCATCCACTTTGTCCACCCGAG-3′; fast troponin I (fTnI), sense: 5′-GAAGCGCAACAGGGCCATCACG-3′, antisense: 5′-CCACGTCACGCAGGTCCCGTTC-3′; Csx/Nkx2.5, sense: 5′-TGGCGTCTGGGGACCTGTCTG-3′, antisense: 5′-GAGTCTGGTCCTGCCGCTGTC-3′; GATA4, sense: 5′-TACATGGCCGACGTGGGAGCA-3′, antisense: 5′-TGGAGTTACCGCTGGAGGCAC-3′; exogeneous GATA4, sense: 5′-CCAGAAAACGGAAGCCCAAGAA-3′ (the sequence derived from mouse GATA4 gene), antisense: 5′-GCTTGCCAAACCTACAGGTGGG-3′ (the sequence derived from pCLPCX vector); adiponectin, sense: 5′-CTGAAGAGCTAGCTCCTGCTTTG-3′, antisense: 5′-GAAGAGAACGGCCTTGTCCTTC-3′; glyceraldehyde-

3-phosphate dehydrogenase (G3PDH), sense: 5′-CCCATCAC-CATCTTCCAGGAGC-3′, antisense: 5′-TTCACCACCTTCTT-GATGTCATCATA-3′. G3PDH was used as an internal control. PCR was performed with TaKaRa Ex-Taq (TAKARA SHUZO CO., LTD) for 30–35 cycles, with each cycle consisting of 94°C for 1 min, 61–68°C for 1 min, and 72°C for 2 min, with an additional 7 min incubation at 72°C after completion of the final cycle.

RT-PCR samples were electrophoresed through agarose gels and stained with ethidium bromide and visualized through a UV light digital imaging system. Densities of electrophoresis bands were analyzed using ScnImage software (Scion Corporation).

Western blot analyses

Western blots were performed using whole-cell extracts according to the standard protocol [27]. Aliquots (30 μg) of whole-cell extracts were electrophoresed in SDS-polyacrylamide gels and transferred onto Immobilon-P polyvinylidene difluoride membrane (Millipore) by electroblotting. After treatment in blocking buffer, membranes were sequentially probed with the antibodies against Nkx2.5 (sc-8697, Santa Cruz) or Gata4 (sc-9053, Santa Cruz), and then with HRP-conjugated anti-goat or rabbit IgG. The bands were revealed using the ECL Plus standard protocol (Amersham Pharmacia Biotechnology).

Cellular transplantation

Following priming by 5-azacytidine for 24 h, the cells were cultured for an additional 3 days. Then the cells were harvested with 0.05% trypsin and 0.25 mM EDTA, and suspended as single cells at a concentration of 1×10^5 cells/μl with PBS. The cell viability in suspension, determined by 0.05% erythrosine dye exclusion, was 90% to 95%. After general anesthesia of the recipient mice by an intraperitoneal injection of 0.05 mg/g body weight pentobarbitone, cell transplantation was performed into the quadrant muscles of syngeneic adult recipient C3H/HeJ mice (CLEA Japan, Inc., Tokyo, Japan), aged 8 to 10 weeks old at a dose of 1×10^6 and 1×10^8 cells per mouse. All animals received humane care in compliance with the "Principles of Laboratory Animal Care" formulated by Keio University School of Medicine and the National Research Institute for Child Health and Development, and the experimental procedures were approved by the Laboratory Animal Care and Use Committee of Keio University School of Medicine.

Histological analyses

Tissues were fixed in 10% neutral buffered formalin and embedded in paraffin. Tissue sections (6 μm) were mounted on poly-L-lysine-coated slides. After deparaffinization with xylene, tissues were rinsed in acetone or ethanol. Slides were incubated in 0.3% H_2O_2 for 30 min. After washing in PBS, tissues were preblocked for 30 min with 5% normal swine serum. They were incubated overnight at 4°C with mouse monoclonal antibody against recombinant GFP (CLONTECH Laboratories, Inc.) diluted 1:500. After rinsing in PBS, the slides were incubated with horseradish peroxidase-conjugated swine anti-mouse immunoglobulin diluted 1:100 with 1% BSA in PBS, and washed in cold PBS. Staining was developed using a solution containing DAB and 0.01% H_2O_2 in 0.05 M Tris–HCl buffer, pH 6.7. Slides were counterstained with hematoxylin. Slices with positive signals for EGFP were further stained

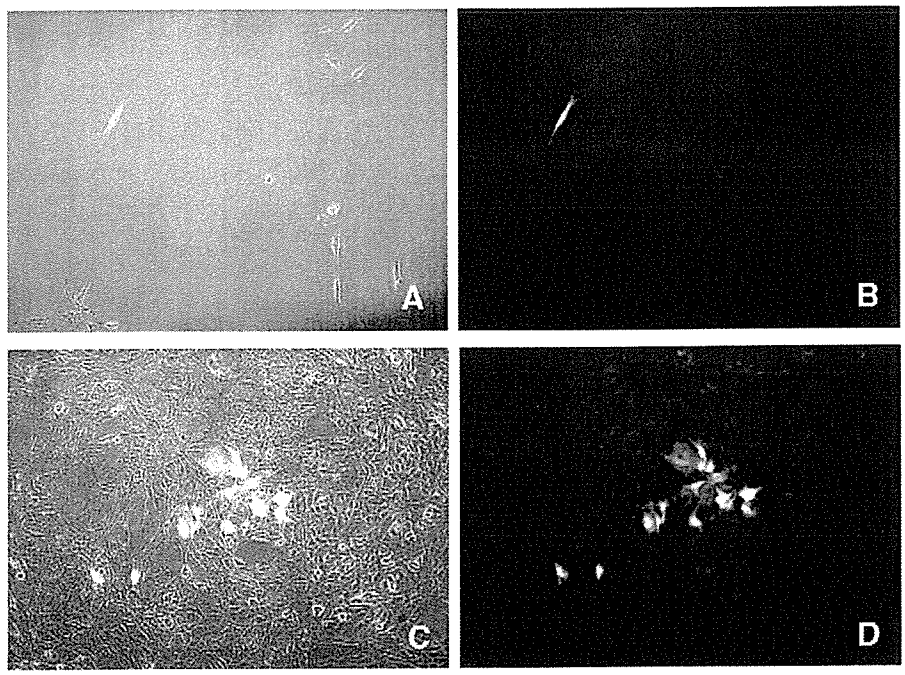

Fig. 1 – Single cell marking by infection of retrovirus carrying EGFP. Phase contrast photomicrograph (A, C) and fluorescent photomicrograph (B, D) of 9-15c cells 1 day (A, B) or 7 days (C, D) after infection with retroviruses carrying EGFP. EGFP-positive single cell-derived cells were clustered.

with anti-CD31 (PECAM-1) antibody (M-20, Santa Cruz Biotechnology, Inc, California, USA).

Frozen sections (6 μm) of the samples were used to detect the donor cells and the differentiation status by examination under a fluorescence microscope. After fixation with acetone and blocking with PBS containing 5% rabbit serum, anti-CD31 or anti-desmin (Bio-Science Products AG, Switzerland) antibodies was used as the first antibody, and rat anti-mouse IgG antibody conjugated with tetramethylrhodamine isothiocyanate (T4280, Sigma, Missouri, USA) and goat anti-mouse IgG antibody conjugated with rhodamine (M116, Leinco Technology, Inc., MO, USA) were used as the second antibody, respectively.

Results

Single-cell marking of 9-15c cells

9-15c cells are mesenchymal stem cells [23,24] capable of differentiating into cardiomyocytes in vitro with the use of 5-azacytidine. To determine if cardiomyocytes were generated from committed cardiac precursor cells or uncommitted stem cells during the differentiation of 9-15c cells, we carried out a single-cell marking experiment. Following retrovirus-mediated EGFP gene infection, a single EGFP-labeled cell could be detected at Day 1 after infection (Figs. 1A, B). The fate of

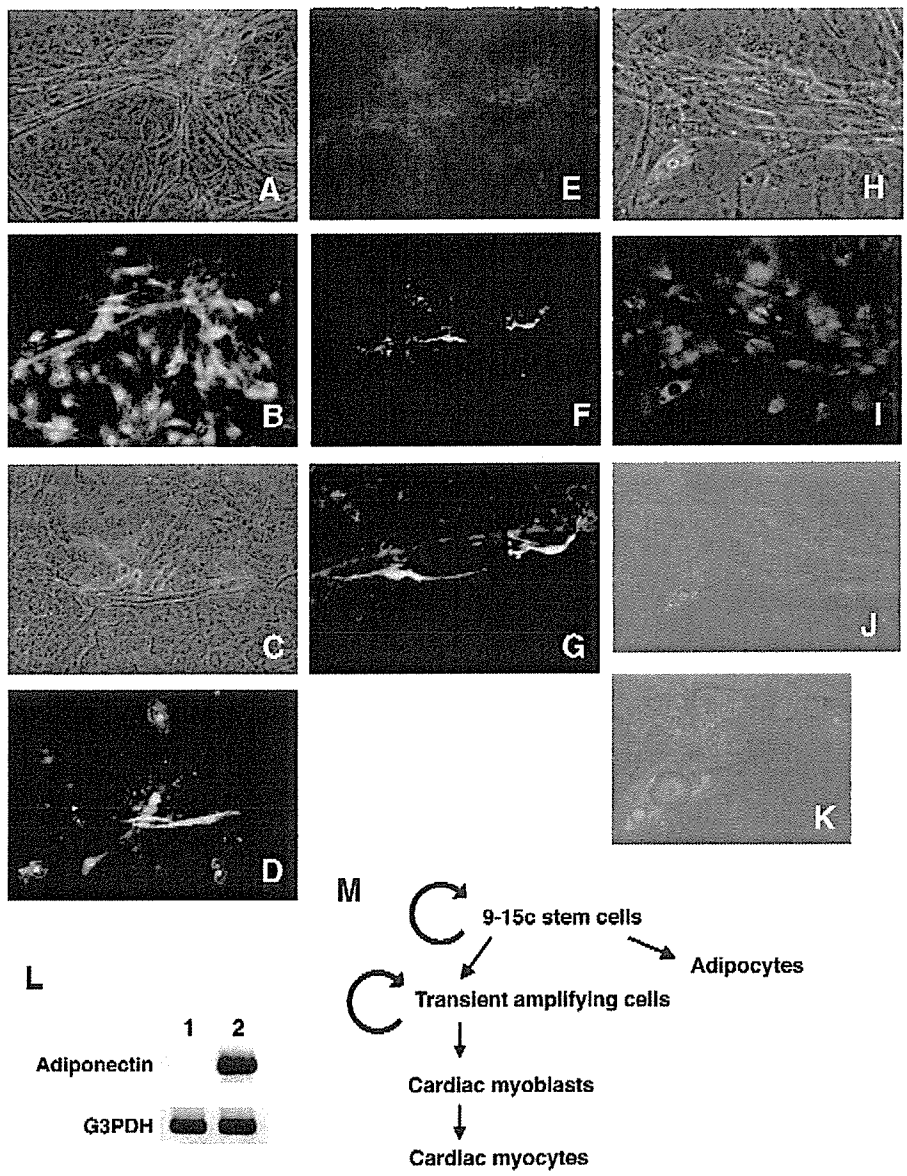

Fig. 2 – Bipotency, i.e., cardiomyogenic and adipogenic differentiation, of single cell-derived cells. Single-cell-derived 9-15c cells marked by EGFP exhibited cardiomyogenic and adipogenic differentiation after exposure to 5-azacytidine. (A–B) Cardiomyogenic and undifferentiated EGFP-marked, single-cell-derived 9-15c cells; (C–G) Cardiomyogenic differentiation of EGFP-marked, single-cell-derived 9-15c cells; (H–J) Cardiomyogenic and adipogenic differentiation of EGFP-marked, single-cell-derived 9-15c cells. (A, C, E, H, J) Phase contrast photomicrographs; (B, D, F, G, I) fluorescent photomicrographs. (K) Enlargement of the panel J. (L) RT-PCR analysis of the adiponectin and G3PDH genes in 9-15c cells at the growing phase without any treatment (lane 1) and 4 weeks after exposure to 5-azacytidine (lane 2). (M) Scheme of 9-15c cell differentiation.

retrovirally tagged 9-15c cells could be traced by monitoring EGFP throughout the differentiation process after exposure to 5-azacytidine. Seven days later, the EGFP-positive, single-cell-derived cells were clustered (Figs. 1C, D). Four weeks after 5-azacytidine treatment, the EGFP-positive cells were examined for differentiated phenotypes. We identified beating cells as cardiomyocytes and oil-red-positive cells as adipocytes. Three kinds of cell populations were observed: a) a cell population in which cardiomyocytes and undifferentiated stem cells were EGFP-positive (Figs. 2A, B); b) a cell population in which all the EGFP-positive cells were cardiomyocytes (Figs. 2C–G); c) a cell population in which cardiomyocytes, adipocytes and undifferentiated stem cells were EGFP-positive (Figs. 2H–K). RT-PCR analysis shows that these cells express adiponectin (Fig. 2L), suggesting the presence of adipocytes among the differentiated population. These results imply that cardiomyocytes are generated from uncommitted stem cells (Fig. 2M).

9-15c multipotent cells were preferentially destined to generate cardiomyocytes by forced expression of transcription factors Csx/Nkx2.5 and GATA4

In order to elucidate the roles of Csx/Nkx2.5 and GATA4 in 9-15c cell differentiation, we infected 9-15c cells with retroviruses carrying Csx/Nkx2.5 and GATA4. We detected Csx/Nkx2.5 and GATA4 gene expression in the infected cell by RT-PCR and Western blotting (Figs. 3A and B). GATA4 gene was originally expressed in 9-15c; we detected the GATA4 transgene with specific primers, but not the endogenous GATA4 gene (Fig. 3A).

Four weeks after the induction of differentiation by 5-azacytidine treatment, we examined the efficiency of cardiomyogenic differentiation or the expression of cardiomyogenic markers. The expression of the ANP and cTnI genes was up-regulated in 9-15c cells overexpressing Csx/Nkx2.5 and GATA4 (9-15c-CG cells) compared to the uninfected 9-15c cells (Fig. 3C, lanes 5 and 9). When 9-15c-CG cells were treated with PDGF and retinoic acid on dishes coated with fibronectin in addition to 5-azacytidine, the expression of the ANP and cTnI gene was further up-regulated (Fig. 3C, lane 10).

Cell implantation into immunodeficient mice

To investigate whether 9-15c-CG cells differentiate in vivo, the cells treated with 10 μM 5-azacytidine for 24 h were injected into immunodeficient mice (Figs. 4A–F). The donor cells clearly formed striated muscles without a branched structure as well as undifferentiated cells 81 days after implantation. The implanted 9-15c-CG cells clearly expressed desmin (Fig. 4G). The grafted cells also generated neovascularization near the injected site 1 month after injection; the EGFP-positive donor cells could be identified as the endothelium of these vessels (Fig. 4H). Immunohistochemistry with an antibody against CD31, a marker for endothelium, confirmed that the donor cells of the newly formed vessels had differentiated into endothelium (Fig. 4Hb). Engrafted donor cells appeared to maintain the characteristics of stem cells, that is, they continued to produce progeny, i.e., differentiated endothelial cells in this case.

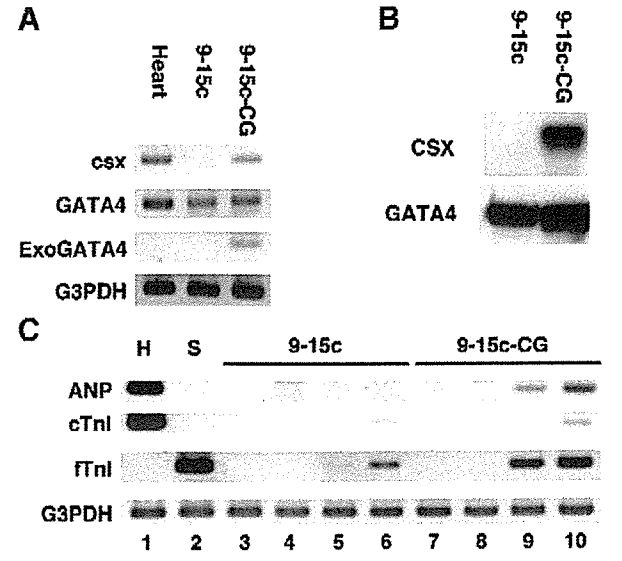

Fig. 3 – Expression of cardiomyocyte-specific or associated genes in 9-15c cells. A: RT-PCR analysis of the Csx, GATA4, exogeneous GATA4 and G3PDH genes (from top to bottom) in adult mouse heart, 9-15c cells and 9-15c cells overexpressing the Csx and GATA4 genes (9-15c-CG cells). B: Western blotting analysis of the Csx and GATA4 proteins in 9-15c cells and 9-15c-CG cells. C: RT-PCR analysis of the ANP, cTnI, and G3PDH genes (from top to bottom) in 9-15c cells (lanes 3–6) and 9-15c-CG cells (lanes 7–10). 9-15c cells (lane 3) and 9-15c-CG cells (lane 7) were cultured without any treatment (lanes 4 and 8) or with exposure to 5-azacytidine alone (lanes 5 and 9), or 5-azacytidine, PDGF, retinoic acid, and fibronectin coating on a dish (lanes 6 and 10) for 4 weeks. Heart (lane 1: H) and skeletal muscle (lane 2: S) served as controls.

Enhancement of cardiomyogenic differentiation by the co-cultivation with cardiomyocytes

We co-cultured EGFP-labeled 9-15c-CG cells with cardiomyocytes of fetal mice in vitro. Four weeks after 5-azacytidine treatment, EGFP-positive beating cardiomyocytes were increased (Figs. 5A, B). To determine whether factors secreted from the cultured cardiomyocytes promoted cardiomyocytic differentiation, 9-15c cells and 9-15c-CG cells were cultured in growth medium supplemented with conditioned medium from cardiomyocyte cultures. The expression of the ANP and cTnI genes was up-regulated in both 9-15c cells and 9-15c-CG cells with exposure to the conditioned medium of cardiomyocyte cultures (Fig. 5C, lanes 3 and 7). Furthermore, treatment with PDGF and retinoic acid, and fibronectin coating on a dish enhanced cardiomyogenic marker expression in both 9-15c cells and 9-15c-CG cells (Fig. 5C, lanes 4 and 8).

Discussion

Different models arise from different conceptions of the MSCs as in hematopoietic stem cells' differentiation [28,29]. A hierarchical model of MSCs has been proposed based on the in vitro differentiation potential of human MSCs as observed